Geochimica et Cosmochimica Acta Vol. 57, pp. 3763–3784
Copyright © 1993 Pergamon Press Ltd. Printed in U.S.A.
0016-7037/93/$6.00 + .00

Refractory inclusions from the Leoville, Efremovka, and Vigarano C3V chondrites: Major element differences between Types A and B, and extraordinary refractory siderophile element compositions

PAUL J. SYLVESTER,[1,*] STEVEN B. SIMON,[1] and LAWRENCE GROSSMAN[1,2]

[1]Department of the Geophysical Sciences, The University of Chicago, Chicago, IL 60637, USA
[2]Enrico Fermi Institute, The University of Chicago, Chicago, IL 60637, USA

(*Received October* 1, 1992; *accepted in revised form February* 2, 1993)

Abstract—We have measured the bulk major and trace element compositions of ten CAIs from Leoville, Efremovka, and Vigarano, members of the reduced subgroup of C3V chondrites, by INAA. Like CAIs from the reduced subgroup studied previously and unlike CAIs from Allende, a member of the oxidized subgroup, nine of the ten CAIs studied here possess only small amounts of secondary phases and, hence, preserve their pre-alteration bulk major element compositions. Using those compositions and model pre-alteration compositions of Allende CAIs, we cannot distinguish Type B1s clearly from B2s, nor some CTAs from FTAs. All Type As and most Type Bs have superchondritic CaO/Al_2O_3 ratios, suggesting that their precursors condensed from a solar gas after ~20% of the Al was removed by high-temperature, Al-rich phases. Type Bs possess higher concentrations of MgO and SiO_2 than do Type As because the precursor phases of Type Bs reacted with the cooling nebular gas to form fassaite, while those of Type As did not.

Eight of the ten CAIs have unusual or unique refractory trace element characteristics compared to those seen in Allende inclusions. Vig1, L2, Ef1, and Ef2 have remarkably high concentrations of Re and Os (~57–145 × C1) because they sampled 4–9 times more hcp condensate metal alloy than did most Allende inclusions. Vig1, L2, Ef1, Ef2, L1, and Vig2 have unusually large Os/Ru ratios (up to 6.9 × C1) because the removal temperatures of their hcp alloy precursors were unusually high (up to ~1655 K at 10^{-3} atm). L2 and L4 have low Zr/Hf ratios (~0.4 × C1); L1 and Ef2, low V/Yb ratios (~0.25 × C1); Ef2, high Th/La (~1.6 × C1), and Sr/Yb (~2.4 × C1) ratios; and Ef3, high Hf/Lu (~2.6 × C1), Sc/Lu (~3.1 × C1), and Zr/Lu (~2.8 × C1) ratios. Most of these fractionations are explained by non-representative nebular sampling of one or more of hibonite, zirconium oxide, perovskite, and melilite, which may be condensates or evaporation residues. Of twenty-five inclusions from the reduced subgroup now studied in this laboratory, seventeen have at least one pair of refractory trace elements which are more fractionated relative to one another compared to C1 chondrites than are the same elements in Allende CAIs, indicating that the host phases of these elements were not as thoroughly mixed together in the nebular region where CAIs of the reduced subgroup accreted as where those in Allende did. Parts of the nebula sampled by C3V chondrites of the reduced subgroup were not well sampled by Allende, and vice versa.

Like most coarse-grained inclusions from the reduced subgroup studied previously, most of those analyzed here have lower concentrations of Na, Au, Fe, Zn, and Mn than their Allende counterparts, consistent with the idea that they experienced secondary alteration at a higher temperature or for a shorter time than did Allende inclusions.

INTRODUCTION

BULK CHEMICAL COMPOSITIONS of Ca-, Al-rich inclusions (CAIs) from carbonaceous chondrites record information about temperatures and oxygen fugacities that existed in the early solar nebula, compositions of oxide, silicate and metal alloy grains that condensed from the nebular gas, and gas-grain fractionations that occurred during condensation. Chemical compositions of many CAIs have been determined, but a large majority of the analyzed inclusions are from Allende, a member of the oxidized subgroup of C3V chondrites (MCSWEEN, 1977). As a result, much of what has been inferred about the early solar nebula is based on compositions of Allende inclusions.

There are two problems with basing so much of our knowledge about the early solar nebula on Allende inclusions without also considering compositions of inclusions from the reduced subgroup of C3V chondrites. First, MACPHERSON et al. (1981), WARK (1981), BECKETT (1986), and MCGUIRE and HASHIMOTO (1989) suggested that, during low-temperature secondary alteration, some Allende inclusions lost CaO and gained SiO_2. In order to obtain information about solar nebular conditions during the earlier, high-temperature stage from the bulk, major element compositions of Allende CAIs, the latter must be corrected for the effects of secondary alteration. This requires knowledge about the compositions and modal abundances of the remaining primary minerals and assumptions about the composition of material that reacted to form alteration products. Although coarse-grained refractory inclusions in the reduced subgroup have nearly identical primary mineral assemblages to those in Allende, the former contain only small amounts of

* *Present address:* Research School of Earth Sciences, The Australian National University, GPO Box 4, Canberra, ACT 2601, Australia.

secondary phases (MACPHERSON et al., 1988). Their primary minerals are so well preserved that the bulk, major element compositions of these inclusions do not have to be corrected for alteration effects.

Second, MAO et al. (1990) and SYLVESTER et al. (1992) found that nine of fifteen CAIs from Leoville and Vigarano, members of the reduced subgroup, have unusual refractory trace element characteristics compared to their mineralogically and petrographically identical counterparts in Allende. This suggests that condensates were distributed heterogeneously in the parts of the solar nebula where C3 chondrites formed, and Leoville and Vigarano inclusions sampled parts of the nebula that were not well sampled by Allende inclusions. It is important, therefore, to continue to search the reduced subgroup for inclusions with unusual refractory trace element compositions in order to gain a more complete knowledge of the range of conditions and processes that led to formation of early nebular materials.

In this paper, we report bulk chemical compositions for ten CAIs from three C3V chondrites of the reduced subgroup, five from Leoville (L1–L5), three from Efremovka (Ef1–Ef3), and two from Vigarano (Vig1 and Vig2), which we measured by instrumental neutron activation analysis (INAA). Six of these inclusions possess very large fractionations between refractory siderophile elements, and four of the six have remarkably high concentrations of those siderophiles, compared to CAIs analyzed previously. Preliminary results of this study were presented by SYLVESTER and GROSSMAN (1991) and SIMON and GROSSMAN (1991).

SAMPLE DESCRIPTIONS

Sawn slabs of Leoville, Efremovka, and Vigarano were acquired from the Field Museum of Natural History. White-colored inclusions are exposed on the surfaces and broken edges of those slabs. Using a microtrimmer in a clean room, fragments of each of ten inclusions were chipped away from their slabs for INAA. Matrix and rust adhering to fragments of some of the inclusions were removed using stainless steel dental tools and forceps. A single chip from the sampled material of each inclusion was made into a polished thin section. For each coarse-grained inclusion, a mineral mode was estimated from a backscattered electron photomosaic of the thin section and, in Table 1, the mode observed in each thin section is compared to a mode calculated from the bulk chemical composition determined here from a split of the same inclusion (discussed later). Petrographic descriptions of all ten of the inclusions are given in the following text.

L1

This is a compact Type A (CTA) inclusion, consisting predominantly of coarse-grained (100–1000 μm), anhedral melilite ($Åk_{20}$–$Åk_{30}$), which encloses minor spinel, perovskite, fassaite, wollastonite, and NiFe metal. Although individual melilite crystals are not zoned, the melilite is extremely gehlenitic ($Åk_5$) near the rim of the inclusion, becoming less so toward the interior. Outward from the gehlenitic zone is a rim sequence of spinel + perovskite, spinel ± hibonite, and an outer layer of melilite ($Åk_{10-20}$) ~20 μm thick. Spinel occurs as isolated, rounded to euhedral grains ~10–60 μm across in the interior of the inclusion and, near the rim, in a fine-grained intergrowth with melilite and perovskite, ± hibonite. Perovskite also occurs in the interior, as isolated, 50–100 μm grains, some of which have ragged boundaries and fassaite rims. An unusual feature of this inclusion is that it contains coarse wollastonite grains, up to ~100 μm across, some of which contain fluffy veinlets of andradite. This inclusion also contains two opaque assemblages, described by SIMON and GROSSMAN (1992), with lamellae of ϵRu-Fe in γNiFe.

Table 1. Comparison of observed and calculated mineral modes for coarse-grained inclusions studied in this work

Inclusion	% melilite		% spinel		% perovskite		% fassaite		% anorthite	
	obs	*calc*	*obs*	*calc*	*obs*	*calc*	*obs*	*calc*	*obs*	*calc*
L1	85	86	10	11	5	4	trace	0	0	0
L2	40	44	18	19	0	0	31	29	11	9
L4	55	61	24	13	0	0	21	26	0	0
L5	65	64	10	12	0	0	10	10	15	14
Ef1	85	89	10	9	1	1.4	2	0	2	0
Ef2	95	95	4	3.4	1	1.0	0	0	trace	0
Ef3	60	68	20	19	0	0	20	12	0	0
Vig1	51	38	29	25	0	0	15	20	5	12
Vig2	57	70	15	16	0	0	28	14	trace	0

L2

This is a typical Type B2 inclusion, 6 × 4.5 mm at the slab surface. It has melilite laths up to 470 μm long and blocky fassaite crystals up to 300 μm across. Fassaite averages 6.6 wt% TiO_2^{tot} (all Ti as TiO_2) and melilite averages $Åk_{39}$. Spinel occurs as euhedral crystals 5–40 μm across, scattered individually or as clumps ~100 μm across within both melilite and fassaite. Anorthite occurs as subhedral crystals 10–150 μm across, typically adjacent to fassaite crystals.

L3

This is an unzoned fine-grained inclusion whose original size was 5 × 2 mm. Spinel grains, which typically are ~10 μm across, enclose micron-sized perovskite grains and have thin (<1 μm) rims of low-Ti (2–6 wt% TiO_2^{tot}) fassaite. These grains are enclosed in a matrix of anorthite + aluminous diopside. Also present in the matrix are rare, 5 μm, rounded grains of melilite ($Åk_{20-25}$), suggesting that melilite may be a primary phase in this fine-grained inclusion. Possibly related to the survival of melilite in L3 is the lack of feldspathoids, which indicates that this inclusion was not subjected to alteration by Na-rich fluid, as were most Allende fine-grained inclusions.

L4

Inclusion L4 was 10 × 3 mm and can be described as a "fluffy" Type A (FTA) (MACPHERSON and GROSSMAN, 1984) that is more compact and less altered than those in Allende. It has a nodular texture, being composed of irregular, rounded bodies ~200–500 μm across. These bodies consist of anhedral melilite grains ($Åk_{7-16}$) <50 μm across which enclose subhedral, 10 μm spinel crystals (both isolated and in clumps ~100 μm across) and minor amounts of anhedral fassaite (10–15 wt% TiO_2^{tot}) up to 20 μm across, fine perovskite, and Os-, Ir-, Pt-bearing NiFe grains up to 10 μm across. The nodules have rims of aluminous diopside which are generally 10–20 μm thick, and in several places meteorite matrix is present between nodules. A few isolated grains of calcite up to ~10 μm across are present in the interior of the CAI, but no Na-bearing phases have been observed.

L5

This is an irregularly shaped, 7 × 3 mm inclusion. It has the mineralogy of a Type B inclusion but an unusual texture and mode. It is melilite-rich (65 vol%) and fassaite-poor (10 vol%) for a Type B, with spinel and anorthite also present. Melilite has been recrystallized forming a mosaic texture in which most grains are 10–30 μm across. Melilite compositions range from $Åk_{15}$–$Åk_{51}$ and average $Åk_{29}$. The melilite is predominantly spinel-free, except at the rim of the inclusion. Most spinel occurs in a layer near the rim and, in the interior, as knots of euhedral, 10 μm crystals enclosed in ~100 μm patches of anhedral fassaite (6–13% TiO_2^{tot}, 16–23% Al_2O_3) or anorthite. Fassaite and melilite are intergrown, but fassaite and anorthite are not. Anorthite invades melilite along cracks and forms patches between grains, poikilitically enclosing small (10 μm), individual melilite crystals. Melilite enclosed in anorthite ranges in shape from rounded to euhedral and in composition from $Åk_{12}$–$Åk_{35}$. This inclusion may have been shocked and reheated after its original crystallization, causing solid-state recrystallization of melilite and melting of anorthite. In addition, it is somewhat deformed, with a lobate protrusion into the matrix and displacement along at least one crack.

Ef1

This is a CTA inclusion, 5.5 × 2.5 mm, dominated by melilite (85 vol%), with spinel and minor perovskite and fassaite. Melilite grains are anhedral, ranging in size from 70–350 μm and in composition from $Åk_7$–$Åk_{28}$. They display wavy extinction and may have been shocked, but are not recrystallized. The inclusion has a rim sequence, from inside to out, of spinel ± perovskite, fassaite, and aluminous diopside. Each layer is approximately 10 μm thick. Inward from the rim there is a 100–200 μm-wide zone of melilite ± perovskite. Further inward, subhedral, rounded spinel grains 10–20 μm across, along with finer-grained perovskite, are present. The inclusion has been fragmented and deformed. In some places, the rim is missing and, in others, it is highly convoluted or even separated from the inclusion by the meteorite matrix. There has been some alteration of melilite to anorthite, mostly near the rim, but no Na-bearing phases are present in this or any of the Efremovka inclusions we studied.

Ef2

This CTA inclusion has the most melilite (95 vol%) and the least spinel and perovskite of the four CTAs in this study. Melilite grains are anhedral to subhedral, 50–560 μm across, somewhat fractured and have wavy extinction. The melilite composition ranges from $Åk_{17}$–$Åk_{35}$, and averages $Åk_{24}$. Spinel occurs as subhedral grains 20–100 μm across, several of which have fine, wormy perovskite grains along their contacts with melilite. Also present are a few isolated, interstitial grains of wollastonite and NiFe metal. No rim structure is present in the polished section. Melilite is in sharp contact with the meteorite matrix along a jagged boundary, suggesting that this is an interior chip of a once-larger inclusion.

Ef3

This inclusion is also a CTA, 4 × 2 mm on the slab surface. In part of it, melilite has been recrystallized to a mosaic of grains, each ~70 μm across, with 120° triple junctions, but elsewhere in the inclusion laths >400 μm long are present. Melilite ranges in composition from $Åk_{11}$ to $Åk_{35}$. There is also a significant amount (~20 vol%) of Ti-rich (18 wt% TiO_2^{tot}) fassaite, which occurs as anhedral crystals 200–300 μm across and poikilitically encloses euhedral spinel crystals. Spinel grains are up to 100 μm across, and many enclose perovskite which is otherwise rare. There are also many NiFe grains, 10–20 μm across, and one large (~100 μm in diameter) object consisting mostly of kamacite, taenite, and phosphate.

Vig1

This CAI, originally a 3 × 2 mm oval at the slab surface, is a Type B2. Fassaite crystals are anhedral, typically 100 μm across, and contain 4–9 wt% TiO_2^{tot}. Some are enclosed in melilite. Spinel occurs as 10 μm, anhedral to subhedral grains enclosed in melilite, fassaite, and anorthite; in framboids, palisades, and palisade bodies (as defined by WARK and LOVERING, 1982); and as rounded crystals up to 50 μm across enclosed in aluminous diopside in the thick (~100 μm) Wark-Lovering rim (WARK and LOVERING, 1977). Melilite has been recrystallized into polygonal grains ~20 μm across, with compositions ranging from $Åk_4$–$Åk_{68}$, and averaging $Åk_{42}$. Numerous 10–20 μm NiFe grains are enclosed in melilite and fassaite. Unlike other inclusions in this study, but like Allende inclusions, Vig1 contains abundant secondary alteration products. These include aluminous diopside, sodalite, and calcite, the latter two phases in 100–200 μm-sized patches in melilite throughout the inclusion. There is also a large reentrant, ~500 μm across, filled with matrix material. Along the reentrant-inclusion contact, the inclusion contains 100 μm patches of Al-diopside and spinel, and discontinuous sections of the Wark-Lovering rim. The many large, irregular patches of Al-diopside, the recrystallized melilite, the reentrant, the clumps of spinel, and the spinel palisades give the inclusion a jumbled texture.

Vig2

This sample is a comma-shaped, 5 × 3 mm fragment of a Type B1 inclusion. The mantle is spinel- and fassaite-rich (14 and 8 vol%, respectively) compared to those in typical Allende B1s, containing anhedral fassaite crystals (with 6–15 wt% TiO_2^{tot}) that are ~100 μm across, and spinel framboids, 50–200 μm across. Melilite is partially recrystallized, with development of 20 μm polygonal subgrains. Unrecrystallized grains are up to 400 μm across. In the mantle, melilite compositions range from ~$Åk_{20}$ at the rim to $Åk_{45-50}$ at the core/mantle boundary. Except for one melilite-rich ($Åk_{36-45}$), spinel-poor island, the inclusion core is extremely fassaite-rich (~60 vol%) and melilite-poor, with coarse (200–500 μm), normally zoned fassaite (3–12 wt% TiO_2^{tot}) and anorthite. The fassaite and minor melilite in the core poikilitically enclose numerous, uniformly distributed, ~10 μm, euhedral spinel crystals. Within the core is a framboid, 450 × 350 μm across, consisting of a ring of relatively coarse (~30 μm), euhedral spinel crystals which encloses melilite ($Åk_{72-74}$), Ti-poor fassaite, spinel, and anorthite. The evolved compositions of minerals in the framboid indicate that it was the last part of the inclusion to crystallize (SIMON and GROSSMAN, 1991). The inclusion has a Wark-Lovering rim, except along the broken edge of the inclusion, where the mantle is in direct contact with the matrix of the meteorite. This indicates that the inclusion was broken after formation of the rim, but before incorporation into the meteorite.

EXPERIMENTAL METHODS

Rabbit Irradiation

Experimental procedures and standards used for the short INAA irradiation, carried out at the University of Missouri Research Reactor (MURR), were the same as those of DAVIS et al. (1982) and SYLVESTER et al. (1992). Each sample was irradiated for 3 min with a neutron flux of 8×10^{13} n/cm^2/sec. Samples and standards were counted twice on one of two 21% efficiency, high-purity Ge detectors at the MURR: first, for 5 min, 2–11 min after irradiation; and next, for 20 min, 4–6 h after irradiation. Neutron flux corrections of ≤3.9% were applied to each sample and standard based on variations in the specific activity of ^{60}Co, assumed to change linearly with time, in Co-doped aluminum wires irradiated during the course of the experiment. Polyethylene pouches into which samples and standards were packaged for irradiation and counting required blank corrections of 0% for Ti, Mg, Ca, and Dy, ≤0.2% for Al, ≤0.9% for V, and ≤4.4% for Mn and Cl. Specpure standards of Al_2O_3 and SiO_2 were used to correct for the fast neutron reactions, $^{27}Al(n, p)^{27}Mg$ and $^{28}Si(n, p)^{28}Al$. Element concentrations measured by INAA are shown in Table 2, which also lists the weight of each sample, and the standard, nuclide, photopeak energy, and half-life used for determination of each element. Errors quoted are 1σ uncertainties due only to counting statistics. Upper limits are based on 2σ uncertainties.

Long Irradiation

Experimental procedures and standards used for the long INAA irradiation were the same as those of MAO et al. (1990) and SYLVESTER et al. (1992). Samples and standards were irradiated and counted in supersilica tubes. The tubes were washed with ultra-pure HCl and HNO_3, double-distilled from Vycor glass, and sealed with a flame fed by filtered oxygen and methane gas. The package of sample, standard, and empty supersilica tubes was irradiated in the flux trap of the MURR for 153 h at a flux of 3.5×10^{14} n/cm^2/sec. After irradiation, each sample was counted three times at the University of Chicago on either of two high-purity Ge detectors with efficiencies of 35.7 and 37.9%: for 1.8–2.7 h, 19–32 h after irradiation; for 6.8–40 h, 2.8–8.3 days after irradiation; and for 6.0–7.0 days, 29–56 days after irradiation.

Data reduction

All corrections applied to the INAA data were made by procedures described in MAO et al. (1990) and SYLVESTER et al. (1992). Corrections for the spatial variation of neutron flux of ≤4% were made to each sample and standard. Lanthanum interference on ^{141}Ce by double neutron capture on ^{139}La, Eu interference on ^{153}Sm by double neutron capture on ^{151}Eu, and Yb interference on ^{177}Lu by decay of reactor-produced ^{177}Yb resulted in corrections amounting to 0.4–0.5%, 0.3–9.1%, and 3.6–23%, respectively, in all samples. Corrections

Table 2. Chemical Compositions of Leoville, Efremovka and Vigarano Inclusions (ppm, unless otherwise noted)

Sample	Description	Mass (μg)	Mass (μg)	CaO (%)	Al_2O_3 (%)	MgO (%)	Na	K	Sc	TiO_2 (%)	V	Cr	Mn	Fe (%)	Co	Ni	Zn	Ga	As (ppb)	Se (ppb)	Br (ppb)	Cl	Sr	Zr
L1	Compact Type A CAI	1158.0 ± 0.1	1157.2 ± 0.1	39.3 ± 1.2	35.8 ± 0.2	5.00 ± 0.15	168 ± 13	31.7 ± 3.6	240.17 ± 0.09	2.19 ± 0.09	407 ± 8	112 ± 1	7.67 ± 0.33	0.044 ± 0.003	7.01 ± 0.02	183 ± 5	< 9.6	< 1.0	91 ± 27	< 250	793 ± 70	< 1200	207 ± 30	131 ± 10
L2	Type B2 CAI	622.1 ± 0.2	621.4 ± 0.1	25.1 ± 1.0	32.7 ± 0.1	10.6 ± 0.3	864 ± 25	47.4 ± 9.7	122.31 ± 0.05	1.68 ± 0.10	702 ± 12	446 ± 4	9.61 ± 0.56	0.106 ± 0.002	0.684 ± 0.017	32.2 ± 5.5	42 ± 12	< 0.99	< 53	580 ± 130	419 ± 41	2030 ± 600	198 ± 23	87.5 ± 8.5
L3	Fine-grained CAI	938.2 ± 0.2	936.3 ± 0.1	12.9 ± 0.8	47.4 ± 0.2	14.6 ± 0.3	641 ± 17	30.5 ± 4.5	91.06 ± 0.02	0.467 ± 0.090	548 ± 14	1258 ± 9	21.1 ± 0.7	0.325 ± 0.002	6.71 ± 0.02	101 ± 4	< 11	< 0.66	< 63	168 ± 34	526 ± 59	< 1500	41.2 ± 6.2	< 9.9
L4	Fluffy Type A CAI	482.1 ± 0.1	481.5 ± 0.1	34.2 ± 1.4	34.7 ± 0.2	7.76 ± 0.30	187 ± 30	18.4 ± 6.2	179.40 ± 0.04	1.79 ± 0.14	834 ± 14	327 ± 3	44.7 ± 1.3	0.547 ± 0.004	38.42 ± 0.05	667 ± 7	< 5.6	< 0.38	80 ± 21	< 130	596 ± 48	< 2700	190 ± 15	53.6 ± 4.9
L5	Type B2 CAI	656.9 ± 0.1	653.3 ± 0.1	32.8 ± 1.2	33.2 ± 0.1	6.90 ± 0.26	263 ± 22	23.4 ± 4.6	90.39 ± 0.02	0.937 ± 0.081	445 ± 9	275 ± 2	6.46 ± 0.41	0.172 ± 0.002	16.45 ± 0.03	406 ± 4	< 5.9	< 0.21	45 ± 17	146 ± 47	< 50	< 100	168 ± 8	54.8 ± 3.5
Ef1	Compact Type A CAI	570.5 ± 0.1	568.0 ± 0.1	37.8 ± 1.4	35.3 ± 0.2	4.13 ± 0.21	197 ± 25	11.3 ± 5.1	104.39 ± 0.02	0.820 ± 0.085	895 ± 15	161 ± 2	12.0 ± 0.7	0.131 ± 0.001	19.18 ± 0.03	562 ± 5	< 6.5	< 0.14	< 29	101 ± 45	826 ± 40	1120 ± 400	211 ± 10	68.8 ± 4.6
Ef2	Compact Type A CAI	224.0 ± 0.1	221.3 ± 0.1	41.3 ± 1.9	29.9 ± 0.1	4.66 ± 0.33	344 ± 65	< 35	54.34 ± 0.01	0.61 ± 0.13	191 ± 8	62.7 ± 2.5	22.9 ± 1.6	0.226 ± 0.005	8.63 ± 0.04	222 ± 12	13.2 ± 4.1	< 0.22	83 ± 22	780 ± 110	89 ± 42	< 4400	253 ± 15	42.2 ± 4.8
Ef3	Compact Type A CAI	1107.7 ± 0.1	1104.1 ± 0.1	30.7 ± 1.0	34.7 ± 0.2	8.66 ± 0.23	258 ± 13	41.3 ± 5.1	294.4 ± 0.1	2.14 ± 0.09	1370 ± 20	320 ± 3	11.6 ± 0.4	1.125 ± 0.008	89.4 ± 0.2	1772 ± 7	18.6 ± 8.3	< 1.1	< 85	< 360	< 160	< 1200	165 ± 22	180 ± 14
Vig1	Type B2 CAI	297.1 ± 0.1	288.8 ± 0.1	26.1 ± 1.4	36.5 ± 0.2	11.8 ± 0.5	2020 ± 50	86 ± 16	124.82 ± 0.03	1.69 ± 0.14	886 ± 16	501 ± 4	26.6 ± 1.5	2.789 ± 0.007	203.1 ± 0.2	4070 ± 11	71 ± 13	< 1.5	< 90	206 ± 86	508 ± 86	< 1200	174 ± 19	86.9 ± 7.0
Vig2	Type B1 CAI	1545.9 ± 0.1	1492.0 ± 0.1	31.1 ± 0.9	25.3 ± 0.1	12.2 ± 0.3	1540 ± 20	20.4 ± 4.6	128.31 ± 0.05	1.18 ± 0.07	807 ± 12	343 ± 3	16.7 ± 0.6	0.500 ± 0.006	30.85 ± 0.06	687 ± 4	22.2 ± 6.6	< 1.0	< 52	< 210	1040 ± 80	390 ± 180	193 ± 19	55.2 ± 5.4
Irradiation[1]		R	L	R	R	R	L	L	L	R	R	L	R	L	L	L	L	L	L	L	L	R	L	L
Nuclide				^{49}Ca	^{28}Al	^{27}Mg	^{24}Na	^{42}K	^{46}Sc	^{51}Ti	^{52}V	^{51}Cr	^{56}Mn	^{59}Fe	^{60}Co	^{58}Co	^{69m}Zn	^{72}Ga	^{76}As	^{75}Se	^{82}Br	^{38}Cl	^{85}Sr	^{95}Zr
Energy (keV)				3084	1779	844	1368	1525	889	320	1434	320	1811	1099	1332	811	439	630	559	265	776	1643	514	757
Half-life				8.72m	2.25m	9.45m	14.97h	12.36h	83.8d	5.76m	3.76m	27.70d	2.579h	44.51d	5.272y	70.91d	13.8h	13.95h	26.3h	119.78d	35.30h	37.2m	64.8d	64.03d
Standard				BCR	Al_2O_3	MgO	SP	SP	SP	TiO_2	BCR	SP	BCR	SP	SP	NZ	NZ	SP	SP	NZ	SP	KCl	BCR	SP
Filomena[2]			84.5 ± 0.1									101 ± 7		96.2 ± 0.2	4820 ±6	50900 ± 70		67.8 ± 2.3	4960 ± 100					
Filomena[3]			168.2 ± 0.2									92.7 ± 3.8		94.1 ± 1.2	4560 ± 10	57060 ± 70		59.0 ± 3.5	5070 ± 120					
Filomena[4]			1409.3 ± 0.2									68.1 ± 1.0		95.7 ± 0.3	4600 ± 20	56400 ± 200			4960 ± 330					
Filomena[5]												68 ± 9			4540 ± 50	56500 ± 600		58.8 ± 1.1	4730 ± 90					
C1 Chondrites[6]				1.30	1.64	16.4	5000	558	5.82	0.0727	56.5	2660	1990	19.04	502	11000	312	10.0	1860	18600	3.57	704	7.80	3.94

[1]Elements determined in the rabbit irradiation are designated by R; in the long irradiation by L. Quoted uncertainties for each concentration are based on 1σ counting statistics errors. [2]This study. [3]SYLVESTER et al. (1992). [4]SYLVESTER et al. (1990). [5]Means and standard deviations of replicate analyses from WASSON et al. (1989), except Os and Ru from PERNICKA and WASSON (1987). [6]ANDERS and GREVESSE (1989). Key to standards: BCR=USGS standard rock BCR-1 (GLADNEY et al., 1983); SP=Standard Pottery (PERLMAN and ASARO, 1969; 1971); Al_2O_3, MgO, TiO_2, KCl= Johnson-Matthey Specpure powders; NZ=Ni, Pd, Pt, Se, Zn solution prepared as in DAVIS et al. (1982); AR=Au, Ir, Re, Os, Ru solution prepared as in MAO et al. (1990); REEA=La, Pr, Eu, Gd, Tb, Ho, Yb solution and REEB=Ce, Nd, Sm, Dy, Er, Tm, Lu solution, both prepared as in EKAMBARAM et al. (1984); W and Mo=SPEX plasma standard solutions.

Table 2 (continued)

Sample	Sb (ppb)	Cs (ppb)	Ba	La	Ce	Sm	Eu	Tb	Dy	Ho	Tm	Yb	Lu	Hf	Ta (ppb)	W	Re	Os	Ir	Mo	Ru	Au (ppb)	Th (ppb)	U (ppb)
L1	61 ± 13	< 32	< 54	5.09 ± 0.04	11.7 ± 0.3	3.16 ± 0.01	1.54 ± 0.01	0.896 ± 0.010	5.98 ± 0.29	1.45 ± 0.06	0.673 ± 0.016	4.72 ± 0.04	0.650 ± 0.008	4.77 ± 0.07	249 ± 10	1.36 ± 0.07	0.844 ± 0.034	11.3 ± 0.1	10.15 ± 0.02	10.7 ± 0.6	11.8 ± 0.2	4.3 ± 1.0	643 ± 20	< 140
L2	< 15	< 25	< 69	5.08 ± 0.02	13.2 ± 0.4	3.23 ± 0.03	1.23 ± 0.01	0.803 ± 0.020	5.31 ± 0.22	1.21 ± 0.16	0.578 ± 0.016	3.84 ± 0.05	0.569 ± 0.018	5.60 ± 0.29	363 ± 10	7.50 ± 0.08	3.87 ± 0.03	53.7 ± 0.2	50.22 ± 0.08	17.4 ± 1.9	47.2 ± 0.2	< 3.2	< 550	134 ± 50
L3	< 12	< 12	< 25	28.9 ± 0.2	64.6 ± 0.1	15.23 ± 0.05	0.312 ± 0.004	2.25 ± 0.01	12.2 ± 0.5	0.847 ± 0.074	1.96 ± 0.01	0.324 ± 0.011	0.0049 ± 0.0020	0.017 ± 0.005	1150 ± 10	< 0.12	< 0.062	< 0.04	0.0057 ± 0.0003	< 0.89	< 0.12	< 1.1	2110 ± 10	< 130
L4	< 19	< 29	< 57	4.49 ± 0.02	11.5 ± 0.2	2.73 ± 0.02	1.411 ± 0.008	0.745 ± 0.017	4.79 ± 0.09	1.13 ± 0.03	0.453 ± 0.017	3.45 ± 0.05	0.443 ± 0.010	3.20 ± 0.13	235 ± 9	1.53 ± 0.06	0.861 ± 0.017	12.84 ± 0.09	11.42 ± 0.01	21.9 ± 1.3	17.6 ± 0.1	< 2.7	534 ± 18	116 ± 41
L5	51.5 ± 6.5	< 16	< 21	2.83 ± 0.02	7.43 ± 0.10	1.734 ± 0.004	1.309 ± 0.006	0.435 ± 0.008	2.73 ± 0.14	0.696 ± 0.018	0.373 ± 0.011	2.50 ± 0.01	0.370 ± 0.003	1.62 ± 0.05	161 ± 5	1.26 ± 0.04	0.499 ± 0.010	8.08 ± 0.03	6.660 ± 0.006	11.9 ± 0.3	10.60 ± 0.06	3.56 ± 0.35	313 ± 8	< 100
Ef1	< 14	< 13	< 28	4.38 ± 0.03	11.2 ± 0.2	2.476 ± 0.007	1.507 ± 0.007	0.617 ± 0.010	4.46 ± 0.09	0.943 ± 0.026	0.385 ± 0.010	2.69 ± 0.02	0.392 ± 0.005	2.17 ± 0.11	204 ± 7	2.47 ± 0.04	4.12 ± 0.03	56.57 ± 0.09	10.42 ± 0.01	15.1 ± 0.6	12.1 ± 0.1	< 1.1	515 ± 19	< 77
Ef2	< 9.3	< 20	< 79	3.20 ± 0.03	8.02 ± 0.24	1.750 ± 0.006	1.449 ± 0.009	0.441 ± 0.013	2.89 ± 0.26	0.690 ± 0.039	0.302 ± 0.019	2.20 ± 0.03	0.317 ± 0.011	1.04 ± 0.03	162 ± 7	2.38 ± 0.05	5.17 ± 0.05	70.4 ± 0.2	54.73 ± 0.05	10.6 ± 1.0	57.9 ± 0.1	2.09 ± 0.53	650 ± 25	< 130
Ef3	< 22	< 25	< 72	3.65 ± 0.03	9.89 ± 0.26	2.392 ± 0.009	1.27 ± 0.01	0.599 ± 0.021	4.06 ± 0.25	0.875 ± 0.054	0.395 ± 0.021	2.61 ± 0.03	0.397 ± 0.010	4.48 ± 0.10	157 ± 15	0.85 ± 0.07	0.528 ± 0.031	7.39 ± 0.11	6.57 ± 0.01	14.3 ± 0.6	10.9 ± 0.2	2.95 ± 0.84	468 ± 24	< 190
Vig1	< 11	55 ± 18	< 44	4.50 ± 0.02	12.2 ± 0.3	2.86 ± 0.01	1.272 ± 0.008	0.714 ± 0.014	4.93 ± 0.28	1.16 ± 0.06	0.492 ± 0.019	3.46 ± 0.04	0.477 ± 0.009	3.01 ± 0.15	224 ± 10	5.25 ± 0.11	2.06 ± 0.02	27.78 ± 0.08	21.04 ± 0.02	37.8 ± 1.3	17.5 ± 0.1	5.0 ± 2.1	497 ± 19	< 130
Vig2	< 12	< 17	< 54	4.04 ± 0.03	10.2 ± 0.2	2.259 ± 0.009	1.226 ± 0.009	0.511 ± 0.011	3.28 ± 0.29	0.784 ± 0.068	0.305 ± 0.007	2.11 ± 0.03	0.312 ± 0.008	1.89 ± 0.06	185 ± 7	1.22 ± 0.06	0.601 ± 0.029	11.0 ± 0.1	8.64 ± 0.01	19.9 ± 0.8	12.75 ± 0.08	2.01 ± 0.61	507 ± 15	< 160
Irradiation[1]	L	L	L	L	L	L	L	L	R	L	L	L	L	L	L	L	L	L	L	L	L	L	L	L
Nuclide	^{124}Sb	^{134}Cs	^{131}Ba	^{140}La	^{141}Ce	^{153}Sm	^{152}Eu	^{160}Tb	^{165}Dy	^{166}Ho	^{170}Tm	^{175}Yb	^{177}Lu	^{181}Hf	^{182}Ta	^{187}W	^{186}Re	^{191}Os	^{192}Ir	^{99}Mo	^{103}Ru	^{198}Au	^{233}Pa	^{239}Np
Energy (keV)	1691	796	373	1596	145	103	1408	879/1178	95	81	84	396	208	482	1221	686	137	129	468	140	497	412	312	278
Half-life	60.20d	2.065y	11.8d	40.28h	32.5d	46.7h	13.4y	72.4d	2.33h	26.8h	129d	4.19d	6.71d	42.4d	114.5d	23.9h	90.7h	15.4d	73.83d	65.94h	39.24d	2.6935d	27.0d	56.4h
Standard	SP	SP	SP	REEA	REEB	REEB	REEA	REEA	SP	REEA	REEB	REEA	REEB	SP	SP	W	AR	AR	AR	Mo	AR	AR	SP	SP
Filomena[2]																2.65 ± 0.27	0.231 ± 0.022	1.20 ± 0.23	3.34 ± 0.01		17.0 ± 1.0	594 ± 26		
Filomena[3]																2.57 ± 0.14	0.264 ± 0.040	0.94 ± 0.20	3.31 ± 0.01		17.9 ± 1.2	613 ± 6		
Filomena[4]																	0.230 ± 0.026	1.06 ± 0.07	3.44 ± 0.03		17.6 ± 0.4	609 ± 4		
Filomena[5]																2.562 ± 0.013	0.234 ± 0.014	1.14 ± 0.13	3.37 ± 0.05		19.3 ± 1.2	612 ± 8		
C1 Chondrites[6]	142	187	2.34	0.2347	0.6032	0.1471	0.056	0.0363	0.2427	0.0556	0.0242	0.1625	0.0243	0.104	14.2	0.0926	0.0365	0.486	0.481	0.928	0.712	140	29.4	8.1

for the overlap of the peak of one nuclide on that of another were based on the ratio of the area of the interfering peak to that of another peak of the same nuclide in a standard. These amounted to 8–20% for ^{182}Ta (84.7 keV) on ^{170}Tm (84.3 keV), 0.2–21% for ^{156}Eu (811.6 keV) on ^{58}Co (810.8 keV), 0.1–5% for ^{152}Eu (810.4 keV) on ^{58}Co (810.8 keV), 0–43% for ^{154}Eu (756.9 keV) on ^{95}Zr (756.7 keV), 0.6–8.5% for ^{169}Yb (130.5 keV) on ^{191}Os (129.4 keV), 0–82% for ^{182}Ta (264.1 keV) on ^{75}Se (264.7 keV), 36–99% for ^{192}Ir (484.6 keV) on ^{181}Hf (482.0 keV), and 0–53% for ^{152}Eu (411.1 keV) on ^{198}Au (411.8 keV). As a consequence of the large neutron fluence of this irradiation, the specific activity of ^{152}Eu in the samples varied from 6% less to 2% more than that of the REE standard, and corrections to the activity of ^{152}Eu in each sample were made accordingly. Holmium was determined by the method of KAWABE et al. (1986): 36–67% of the total ^{166}Ho counts in all samples were due to second-order activation of ^{164}Dy, and appropriate corrections were made.

Blank corrections

Blank corrections were calculated from the mean amount of each element of interest present in four empty supersilica tubes prepared in the same way as, and irradiated along with, the tubes containing the samples. Standard deviations of the means of elements in the empty tubes are <35% of those means, except for Cr (41%), Ni (44%), Na (48%), and Fe (48%). Blank corrections were <0.3% of the amount present for La, Ce, Sm, Eu, Tb, Ho, Tm, Yb, Lu, Re, Os, Ir, Ru, Mo, Th, U, Zr, Sc, Ba, As, Ga, Se, Cs, Br, Sr, and Hf (except 8% in L3) in all samples. Blank corrections were <1% of the amount present for Co (except 5% in L2), Cr (except 5% in Ef2), and Fe; ≤3% for Ni (except 4% in Ef2, 9% in L2), Ta (except 6% in Ef2), Au (except 9% in Ef2), and Zn (except 16% in Ef2); <4% for W; <5% for Sb; <10% for Na (except 12% in Ef1, 15% in L4, and 17% in Ef2); and 12–49% for K in all samples. Corrections for Cr, Ta, Au, Zn, and Na in Ef2 are larger than in other samples because the sample weight of Ef2 is smaller than the weights of all other samples.

Filomena

A small aliquant (84.5 μg) of the IIAB hexahedrite, Filomena, was included in the long irradiation as a secondary standard. Concentrations of Fe, As, W, Re, Os, Ir, Ru, and Au determined here are within 2σ of those measured previously in this laboratory on 1.4 mg (SYLVESTER et al., 1990) and 168 μg (SYLVESTER et al., 1992) samples of Filomena. Concentrations of As, W, Re, Os, Ir, Ru, and Au are also within 2σ of the means of these elements in replicate analyses of Filomena by PERNICKA and WASSON (1987) and WASSON et al. (1989). Concentrations of Co and Ni measured here, however, are significantly larger and smaller, respectively, than in the previous determinations of those elements, and concentrations of Cr and Ga are within 2σ of those measured previously in only the 168 μg sample. These results indicate that heterogeneities in the concentrations of Fe, As, W, Re, Os, Ir, Ru, and Au in Filomena that are seen when only 84.5 μg are analyzed are smaller than the uncertainties of INAA, but this is not so for heterogeneities in Cr, Co, Ni, and Ga. Chromium heterogeneities in Filomena have been seen previously in larger samples than that analyzed here, and may be the result of nonrepresentative sampling of daubreelite (WASSON et al., 1989; SYLVESTER et al., 1992).

MAJOR ELEMENTS

Calculated Mineral Modes and Nonrepresentative Sampling

Because melilite, fassaite, spinel, and other minerals are distributed heterogeneously within coarse-grained CAIs and because we performed INAA on fragments of CAIs, not whole inclusions, there is uncertainty as to whether those fragments have compositions representative of the inclusions from which they are derived. We examined this by calculating a modal mineralogical composition for the sample of each of the nine coarse-grained inclusions analyzed using its bulk major element (CaO, Al_2O_3, TiO_2, MgO) composition, as determined by INAA, and the compositions of its constituent minerals, as determined by electron microprobe analysis. Weighted average compositions were used for pyroxene and melilite, phases exhibiting variable composition. For this calculation, the concentration of silica in each inclusion is determined by difference, which is probably a very good estimate of the actual concentration, because silica is the only major or minor element oxide not determined by INAA. Calculated modal abundances are compared to observed modal abundances in Table 1. There are good matches for L1, L2, L5, Ef1, and Ef2, but the results for L4, Ef3, Vig1, and Vig2 are discrepant. While it is possible that the analyzed sample, the thin section, or both are not representative of the bulk inclusion, a good match suggests that the INAA sample is representative. Poor matches are obviously suspect.

For L4, the INAA sample is poorer in spinel and slightly richer in melilite and fassaite than its corresponding thin section, and for Vig1, the INAA sample is poorer in melilite and richer in fassaite and anorthite than its thin section sample. For Vig2 and Ef3, the INAA samples are poorer in fassaite and richer in melilite than their corresponding samples in thin section. Spinel forms large clumps in L4, as just described, and the thin section sample of that inclusion probably possesses a larger proportion of those clumps than does the INAA sample. The entire discrepancy for Vig2, a Type B1 inclusion with a melilite-rich mantle and a fassaite-rich core, can be accounted for if the INAA sample has a weight ratio of mantle to core (~87:13) that is larger than that of the thin section sample (~60:40).

Bulk Compositions of Coarse-Grained CAIs from C3V Chondrites

There are two first-order questions about bulk major element compositions of coarse-grained refractory inclusions from C3V chondrites (e.g., GROSSMAN, 1980). Are compositions of Type A (melilite-rich) inclusions the same as those of Type B (fassaite-rich) inclusions? Are compositions of both kinds of inclusions the same as those predicted from thermodynamic data for condensate assemblages from a cooling solar nebula gas? Neither question has been answered unambiguously using major element analyses of refractory inclusions from Allende. This is because Allende inclusions contain large amounts of low-temperature, secondary alteration products, such as anorthite, grossular, and nepheline, which typically comprise ~70 vol% of fluffy Type As and ~25 vol% of compact Type As and Type Bs (BECKETT, 1986). Petrographic studies of mineral layers in the rims of coarse-grained (MACPHERSON et al., 1981), and in the cores and rims of fine-grained (MCGUIRE and HASHIMOTO, 1989), Allende inclusions suggest that the secondary phases formed by reaction of primary phases, largely melilite, with Si, Fe, and Na from the nebular gas, possibly resulting in loss of Ca. Thus, the present bulk compositions of Allende inclusions are not the same as the primary bulk compositions, and for each inclusion the precise changes in bulk composition caused by alteration are not known.

WARK (1981) and BECKETT (1986) recognized that Allende inclusions do not preserve their primary bulk compositions and, hence, calculated pre-alteration compositions for those inclusions by making assumptions about the composition of material that was altered to form secondary phases. An alternative approach to determination of the primary compositions of Types A and B inclusions, which is adopted here and which does not require calculation of model compositions, is to use major element analyses of refractory inclusions from the reduced subgroup of C3V chondrites. The present bulk compositions of inclusions from the reduced subgroup are probably very similar to their primary compositions, because secondary mineral phases are much less abundant in these CAIs than in Allende inclusions (MACPHERSON et al., 1988).

Composition differences between Type A and Type B inclusions

Table 3 lists the means and standard deviations of the means of concentrations and ratios of major element oxides in Type A and Type B CAIs from C3V chondrites. Hibonite-rich (>20–30%), melilite + spinel inclusions, which have been found in Allende (WARK, 1981; WARK and BOYNTON, 1983; WARK, 1986) and which WARK (1981; 1986) classified as Type As, are not included in this compilation because they are so different in composition from Type As, as defined by GROSSMAN (1975), which contain only minor amounts of hibonite. In Table 3, compositions of altered inclusions from Allende and of less altered inclusions from Efremovka, Leoville, and Vigarano, members of the reduced subgroup, are taken from this study, unpublished work from our laboratory, and various literature sources. Each composition was determined by either neutron activation analysis of chips and powders of CAIs, or electron microprobe analyses of polished thin sections or fused glasses made from pieces of CAIs.

Model, pre-alteration, bulk compositions of Allende inclusions from WARK (1981) and BECKETT (1986) are also shown in Table 3. BECKETT (1986) calculated bulk compositions for eight Type A and nine Type B Allende inclusions using compositions and modal abundances of melilite, spinel, perovskite, and hibonite in each Type A, and melilite, fassaite, spinel, and anorthite in each Type B. In the calculation, the mean composition of each phase in each inclusion was determined by electron microprobe analysis, except in the cases of spinel, anorthite, and perovskite, for which stoichiometric compositions were used. Modal abundances of the phases were determined by point counting. As mentioned, petrographic observations of coarse-grained Allende CAIs (e.g., MACPHERSON et al., 1981) indicate that the amount of secondary phases formed at the expense of melilite is much greater than that formed from other primary phases. Thus, in BECKETT's (1986) calculation of bulk inclusion compositions, the amount of secondary phases now present is replaced by an equivalent amount of melilite and included spinel with the same bulk composition as unaltered melilite and included spinel in that inclusion.

WARK (1981) calculated model pre-alteration bulk compositions for four Type A Allende inclusions from data obtained by manually rastering a 30 μm-wide electron microprobe beam over representative areas of a polished thin section of each. Using this bulk composition, and mean compositions of all primary and secondary phases determined by electron microprobe analysis, he calculated the proportions of those phases and the bulk compositions of the primary phases and of the secondary phases. Like BECKETT (1986), WARK (1981) assumed that secondary phases in Type A inclusions were derived from melilite having the same composition as unaltered melilite in those inclusions but, unlike BECKETT (1986), he did not assume that the amounts of secondary phases now present formed from equivalent amounts of melilite. Instead, WARK (1981) assumed that Al_2O_3 was the only major element oxide to have remained immobile during alteration, an assumption which has been challenged by HASHIMOTO (1992), and, thus, the amount of melilite converted to secondary phases is that which has the same amount of Al_2O_3 as the bulk composition of those secondary phases. Despite their different methods of calculation, WARK's (1981) and BECKETT's (1986) mean compositions of pre-alteration Type A Allende inclusions are within error of each other. Thus, in order to derive the mean for pre-alteration Type As listed in Table 3, compositions of all twelve of their model Type A inclusions have been averaged together.

Table 3 shows that model pre-alteration Type A Allende inclusions have lower mean SiO_2 (22.8 ± 0.7 wt%) concentrations than do altered Allende Type As (27.7 ± 1.5 wt% SiO_2), as was noted by WARK (1981), and higher mean CaO concentrations, 36.9 ± 0.5 vs. 28.3 ± 1.6 wt% CaO, as was noted by WARK (1981) and BECKETT (1986).

In contrast to Type A inclusions, Table 3 shows that the

Table 3. Means and standard deviations of the means of concentrations (wt %) and ratios of major element oxides in CAIs from C3V chondrites

	<---------Type As--------->			<---------Type Bs--------->		
	Allende[1]	Pre-alteration Allende[2]	Reduced Subgroup[3]	Allende[4]	Pre-alteration Allende[5]	Reduced Subgroup[6]
n	11	12	8	26	9	13
SiO_2	27.7 ± 1.5	22.8 ± 0.7	22.2 ± 1.4	29.9 ± 0.6	28.6 ± 1.1	27.3 ± 1.1
TiO_2	1.42 ± 0.22	1.21 ± 0.24	1.59 ± 0.24	1.33 ± 0.05	2.02 ± 0.17	1.61 ± 0.14
Al_2O_3	34.9 ± 1.9	34.1 ± 1.1	33.2 ± 1.6	29.0 ± 0.6	31.1 ± 1.5	32.2 ± 1.2
FeO	1.51 ± 0.22	0.04 ± 0.02	0.56 ± 0.18	0.78 ± 0.08	0.03 ± 0.01	0.54 ± 0.09
MgO	5.06 ± 0.97	4.91 ± 0.61	5.77 ± 0.73	10.9 ± 0.5	10.6 ± 0.8	11.9 ± 0.7
CaO	28.3 ± 1.6	36.9 ± 0.5	36.5 ± 1.3	27.6 ± 0.7	27.8 ± 1.4	26.3 ± 1.2
Na_2O	0.94 ± 0.19	—	0.05 ± 0.01	0.32 ± 0.07	—	0.11 ± 0.02
CaO/Al_2O_3	0.849 ± 0.077	1.10 ± 0.05	1.13 ± 0.09	0.962 ± 0.031	0.923 ± 0.078	0.840 ± 0.062
MgO/Al_2O_3	0.144 ± 0.026	0.150 ± 0.023	0.177 ± 0.022	0.378 ± 0.019	0.342 ± 0.019	0.374 ± 0.023
TiO_2/Al_2O_3	0.042 ± 0.007	0.035 ± 0.007	0.048 ± 0.007	0.046 ± 0.002	0.065 ± 0.005	0.050 ± 0.003
SiO_2/Al_2O_3	0.841 ± 0.089	0.687 ± 0.049	0.702 ± 0.098	1.05 ± 0.04	0.950 ± 0.075	0.876 ± 0.073

Note: n=number of samples.

Data sources: (1) GRAY and COMPSTON (1974), DAVIS et al. (1978), WARK (1981), GROSSMAN (unpublished); (2) WARK (1981), BECKETT (1986); (3) NAZAROV et al. (1982), MAO et al. (1990), SYLVESTER et al. (1992), this study; (4) GRAHAM (1975), CONARD (1976), WARK and LOVERING (1982), GROSSMAN (unpublished); (5) BECKETT (1986); (6) As in (3), plus PALME and WLOTZKA (1979), WARK and LOVERING (1982). Vigl of this study is not included in (6) because it contains large amounts of secondary phases.

mean SiO_2 (28.6 ± 1.1 wt%) and CaO (27.8 ± 1.4 wt%) concentrations of model pre-alteration Type B Allende inclusions are not very different from those of altered Allende Type Bs (29.9 ± 0.6 wt% SiO_2 and 27.6 ± 0.7 wt% CaO). This observation has not been noted previously and suggests that the amounts of SiO_2 gained and CaO lost during low-temperature secondary alteration of Type Bs, in contrast to Type As, are smaller than the errors of the methods employed to estimate them. This is presumably because melilite is much less abundant in Type Bs than in Type As, and because fassaite, a major Si- and Ca-bearing phase in Type Bs, is not extensively converted to alteration products.

BECKETT (1986) noted that model pre-alteration Type A Allende inclusions have bulk compositions that differ from those of their Type B counterparts. As can be seen in Table 3, compared to the model Type Bs, model Type As have a higher mean CaO (36.9 ± 0.5 vs. 27.8 ± 1.4 wt%) concentration, lower mean SiO_2 (22.8 ± 0.7 vs. 28.6 ± 1.1 wt%) and MgO (4.9 ± 0.6 vs. 10.6 ± 0.8 wt%) concentrations and lower mean SiO_2/Al_2O_3 (0.69 ± 0.05 vs. 0.95 ± 0.08), TiO_2/Al_2O_3 (0.035 ± 0.007 vs. 0.065 ± 0.005), and MgO/Al_2O_3 (0.150 ± 0.023 vs. 0.342 ± 0.019) ratios.

Compositions of Type A and Type B inclusions from the reduced subgroup are similar to the model pre-alteration compositions of their Allende counterparts. In Table 3, concentrations of SiO_2, TiO_2, Al_2O_3, MgO, and CaO in Type As of the reduced subgroup are all within 1σ of those in the model Allende Type As, and concentrations of SiO_2, Al_2O_3, MgO, and CaO in Type Bs of the reduced subgroup are within 1σ (2σ for TiO_2) of those in the model Allende Type Bs. This also holds true if those samples thought not to be representative of their whole inclusions in MAO et al. (1990), SYLVESTER et al. (1992), and this study are omitted from the compilation. Excluding those samples, the mean composition of six Type As from the reduced subgroup is 22.5 ± 1.9 wt% SiO_2, 1.46 ± 0.31 wt% TiO_2, 32.7 ± 2.2 wt% Al_2O_3, 5.0 ± 0.7 wt% MgO, and 37.8 ± 1.2 wt% CaO, and the mean of seven Type Bs from the reduced subgroup is 29.2 ± 1.4 wt% SiO_2, 1.44 ± 0.18 wt% TiO_2, 31.9 ± 1.7 wt% Al_2O_3, 11.1 ± 0.8 wt% MgO, and 25.5 ± 1.7 wt% CaO.

The discovery that compositions of Types A and B inclusions from the reduced subgroup are very similar to the compositions of their model pre-alteration Allende counterparts is important for two reasons. First, it suggests that any errors introduced by the methods of WARK (1981) and BECKETT (1986) for computing the pre-alteration compositions of CAIs from the bulk compositions of altered Allende inclusions are small. Second, it seems to confirm the idea, derived from model compositions of Allende inclusions, that Type A inclusions are richer in CaO and poorer in SiO_2 and MgO than Type B inclusions, and those differences reflect nebular processes that occurred before low-temperature secondary alteration.

Composition differences between FTAs, CTAs, Type B1s, and Type B2s

Type A and Type B inclusions from C3V chondrites are divided into petrographic subtypes called fluffy Type As, compact Type As, Type B1s, and Type B2s. Both FTAs and CTAs consist of melilite and some spinel with minor hibonite and perovskite, but CTAs are spherical, probably once-molten objects, like Type B inclusions, whereas FTAs have convoluted shapes and are thought to be unmelted, nebular condensates (MACPHERSON and GROSSMAN, 1984). Type B1s are concentrically zoned, with a thick melilite-rich mantle surrounding a core of fassaite, melilite, spinel, and anorthite; Type B2s have the same mineralogy as Type B1s but lack a melilite-rich outer rind (WARK and LOVERING, 1982).

Using model pre-alteration compositions of Allende inclusions, BECKETT (1986) found that four FTAs have lower MgO and SiO_2 and higher Al_2O_3 concentrations than four CTAs. He suggested, therefore, that CTAs are not simply the melting and recrystallization products of FTAs, and that CTAs formed or evolved under nebular conditions which differed from those for FTAs. In fact, however, the mean concentrations of MgO (4.1 ± 0.7 wt%), SiO_2 (21.5 ± 1.0 wt%), and Al_2O_3 (36.6 ± 1.4 wt%) in the FTAs of BECKETT (1986) are within 2σ errors of those in his CTAs (7.1 ± 1.1 wt% MgO, 25.3 ± 1.2 wt% SiO_2, 30.4 ± 2.1 wt% Al_2O_3). BECKETT (1986) also found that three model Allende Type B1s have lower mean MgO (8.24 ± 0.30 wt%) and higher mean CaO (31.8 ± 1.0 wt%) concentrations than six model Allende Type B2s (11.8 ± 0.8 wt% MgO, 25.8 ± 1.5 wt% CaO), a difference he ascribed to a larger proportion of fassaite in the condensate precursors of Type B2s than in those of Type B1s. WARK and LOVERING (1982), using the bulk compositions of seventeen Type Bs, fifteen being altered inclusions from Allende, reported that twelve Type B1s have lower MgO and higher CaO concentrations than five Type B2s. They suggested that Type B inclusions are evaporation residues of nebular dust, and Type B1s were heated to higher temperatures and, hence, have undergone more evaporation than Type B2s. In fact, however, the mean MgO (10.2 ± 0.4 wt%) and CaO (28.8 ± 0.6 wt%) contents of the Type B1s of WARK and LOVERING (1982) are within 2σ errors of those of their Type B2s (11.5 ± 1.2 wt% MgO, 25.9 ± 1.2 wt% CaO).

From the data for model Allende and reduced subgroup inclusions used to compile Table 3, we now re-examine whether the differences in composition between FTAs and CTAs, and between Types B1 and B2, suggested by BECKETT (1986) in model Allende inclusions, persist in an expanded data base. We find no difference between FTAs and CTAs in mean CaO (36.3 ± 0.8 vs. 36.9 ± 1.0 wt%) or TiO_2 (1.36 ± 0.19 vs. 1.27 ± 0.24 wt%) concentrations, or between Types B1 and B2 in mean SiO_2 (27.0 ± 1.2 vs. 27.1 ± 1.1 wt%), TiO_2 (1.85 ± 0.19 vs. 1.79 ± 0.13 wt%) or Al_2O_3 (30.8 ± 1.3 vs. 32.5 ± 1.2 wt%) concentrations. From the data used for Table 3, we have plotted the concentrations of SiO_2 vs. Al_2O_3, MgO vs. Al_2O_3, and CaO vs. Al_2O_3 for FTAs and CTAs in Fig. 1, and MgO vs. CaO, SiO_2 vs. CaO, and Al_2O_3 vs. CaO for Types B1 and B2 in Fig. 2. In the Type A comparisons, the model Allende inclusion data of WARK (1981) were omitted because he did not distinguish between FTAs and CTAs. In the Type B comparisons, the reduced subgroup data of NAZAROV et al. (1982) were omitted because they did not distinguish between Types B1 and B2.

Figure 1 indicates that, for both model Allende inclusions and inclusions from the reduced subgroup, FTAs generally fall within much tighter clusters on oxide-oxide plots than

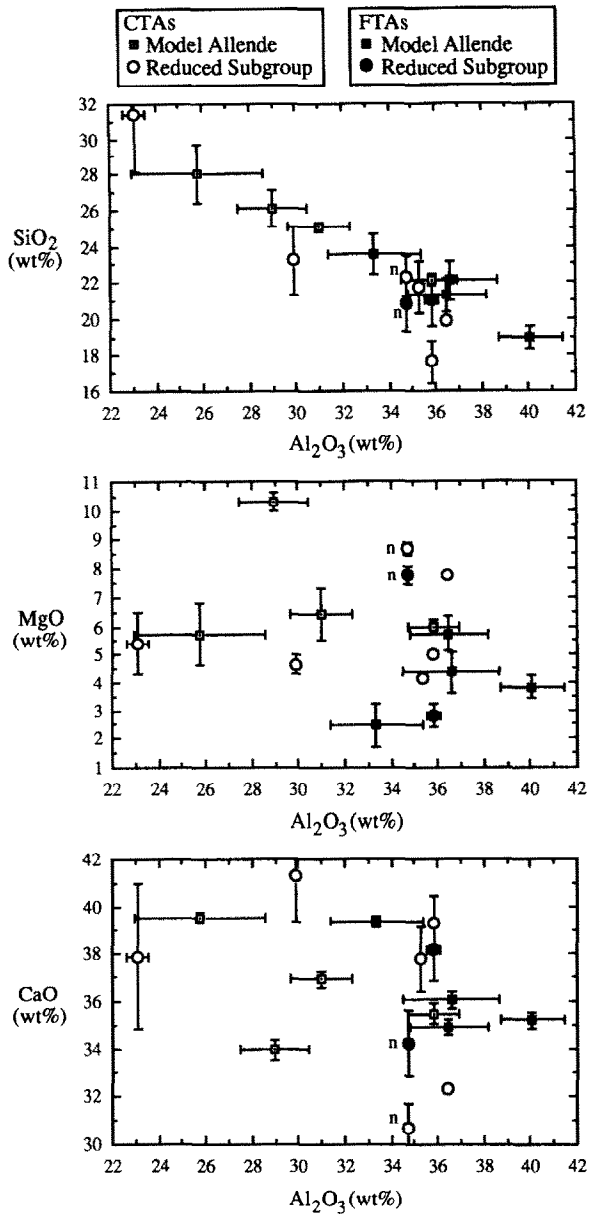

FIG. 1. Comparison of SiO_2 vs. Al_2O_3, MgO vs. Al_2O_3, and CaO vs. Al_2O_3 in model Allende and reduced subgroup CTAs and FTAs. 1σ error bars shown where larger than plotted symbols. Data points for possibly nonrepresentative samples marked by "n".

CTAs. Furthermore, although some CTAs have lower Al_2O_3 and higher SiO_2 contents than do FTAs, as noted by BECKETT (1986), other CTAs have nearly identical Al_2O_3 and SiO_2 contents to the FTAs. In fact, two of the latter CTAs are inseparable from the FTA cluster on all other oxide-oxide plots. The latter CTAs, therefore, could simply be the solidification products of whole melts of FTAs. The low-Al_2O_3, high-SiO_2 CTAs, however, must have melted from assemblages of nebular condensates which had compositions that differed from those of FTAs. The foregoing results are not changed if inclusions which may be nonrepresentative samples (labelled "n" in Fig. 1) are excluded from consideration.

In Fig. 2, there are simply too few samples in each category to determine whether any real differences exist between model Allende and reduced subgroup Type B1s or between model Allende and reduced subgroup Type B2s, particularly when possibly nonrepresentative samples are neglected. Figure 2 does indicate, however, that the ranges of MgO, SiO_2, Al_2O_3, and CaO concentrations in Type B1 inclusions almost completely overlap those in Type B2 inclusions. Both inclusion types have similar interelement relationships, with negative correlations between MgO and CaO and between Al_2O_3 and CaO, and a positive correlation between SiO_2 and CaO. Because of the concentric zonation of the mineral assemblage that is characteristic of Type B1 inclusions, the latter are notoriously difficult to sample properly, especially by means of a single thin section (BECKETT, 1986). Because Type B1 mantles are composed predominantly of melilite and their cores of fassaite and spinel, a series of samples containing

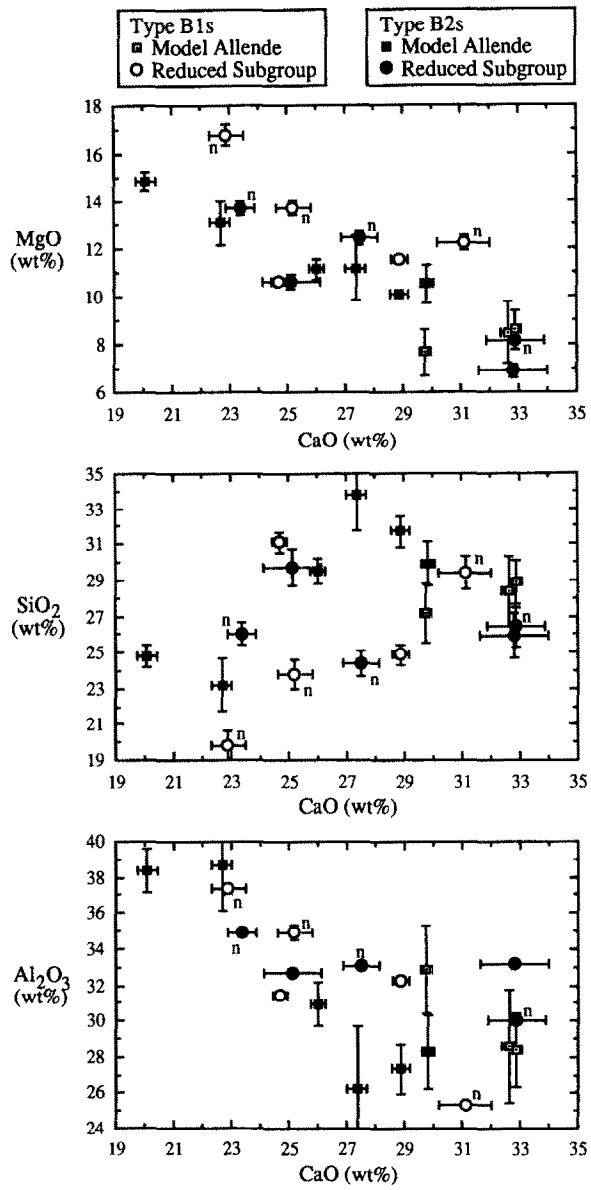

FIG. 2. Comparison of MgO vs. CaO, SiO_2 vs. CaO, and Al_2O_3 vs. CaO in model Allende and reduced subgroup Type B1s and Type B2s. 1σ error bars shown where larger than plotted symbols. Data points for possibly nonrepresentative samples marked by "n".

different proportions of the core and mantle of a single Type B1 inclusion would be almost invariant in SiO_2 and Al_2O_3 while displaying a 50% variation in CaO concentration. The fact that a very good positive correlation between SiO_2 and CaO and a very good negative correlation between Al_2O_3 and CaO are found for the Type B1 inclusions in Fig. 2 suggests that this particular kind of nonrepresentative sampling has not had a major effect on their bulk compositions. At least one Type B1-Type B2 pair can be identified (at ~25 wt% CaO) in which the two inclusions have nearly identical MgO, SiO_2, Al_2O_3, and CaO contents. This would seem to indicate that there are no systematic major element differences between Types B1 and B2, contradicting the suggestion of BECKETT (1986) that the condensate precursors of Type B1s contained a smaller proportion of fassaite than those of Type B2s, and the idea of WARK and LOVERING (1982) that Type B1s are more evaporated than Type B2s. Unfortunately, a relatively large number of data points (labelled "n" in Fig. 2) are from possibly nonrepresentative samples. When the latter samples are omitted from consideration, the degree of overlap on Fig. 2 decreases. The average concentrations in the remaining Types B1 and B2 are MgO, 9.4 ± 0.7 and 11.0 ± 0.8; CaO, 29.8 ± 1.5 and 26.6 ± 1.4; SiO_2, 28.1 ± 1.0 and 28.6 ± 1.3; Al_2O_3, 30.7 ± 0.9 and 32.0 ± 1.7 wt%, respectively. These averages are either within or just beyond 1σ uncertainties from one another for all oxides, further indicating that there is no strong case to be made for differences in composition between Type B1s and Type B2s.

Comparisons with calculated condensate compositions

In a gas of solar composition, Al is slightly more refractory than Ti and both are more refractory than Ca. All three elements are much more refractory than Mg and Si. Calculations describing equilibrium condensation from a cooling solar gas at a total pressure of 10^{-3} atm suggest that, by ~1600 K, all of the Al and Ti in the gas has condensed; by ~1550 K, 90% of the Ca has condensed; but, by ~1450 K, only small fractions of the Mg and Si have condensed (GROSSMAN, 1972, 1977). Model condensate mixtures which stopped equilibrating with the nebular gas at temperatures greater than ~1600 K have subchondritic CaO/Al_2O_3 and TiO_2/Al_2O_3 ratios but, at equilibration temperatures less than ~1550 K, the condensates have nearly chondritic CaO/Al_2O_3 and TiO_2/Al_2O_3 ratios. At all temperatures above 1450 K, the model condensates have strongly subchondritic MgO/Al_2O_3 and SiO_2/Al_2O_3 ratios.

Figure 3 is a plot of CaO/Al_2O_3 vs. TiO_2/Al_2O_3 ratios of inclusions from the reduced subgroup and of the model pre-alteration Allende inclusions of BECKETT (1986) used in compiling Table 3. None of the inclusions plotted have subchondritic CaO/Al_2O_3 and TiO_2/Al_2O_3 ratios, as expected for very high-temperature (>1600 K) equilibrium condensates, or chondritic CaO/Al_2O_3 and TiO_2/Al_2O_3 ratios, as expected for somewhat lower temperature (<1550 K) equilibrium condensates. Instead, most inclusions have superchondritic CaO/Al_2O_3 ratios and, in those, TiO_2/Al_2O_3 ratios range from subchondritic to superchondritic. Most inclusions with subchondritic TiO_2/Al_2O_3 ratios are Type As while most with superchondritic TiO_2/Al_2O_3 ratios are Type Bs. These

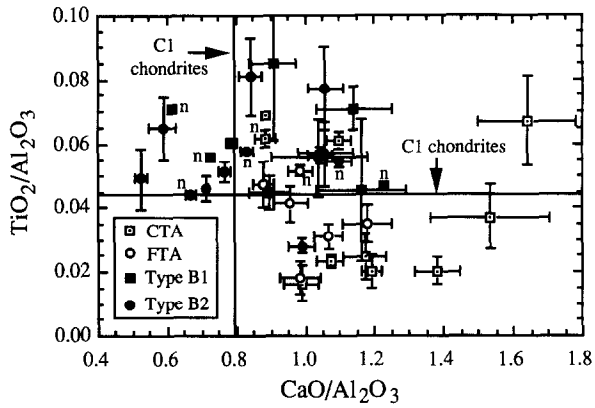

FIG. 3. CaO/Al_2O_3 vs. TiO_2/Al_2O_3 ratios of model Allende and reduced subgroup CTAs, FTAs, Type B1s, and Type B2s. Ratios in C1 chondrites are indicated by reference lines. 1σ error bars shown where larger than plotted symbols. Data points for possibly nonrepresentative samples marked by "n".

generalizations are valid whether or not the possibly nonrepresentative samples are included.

BECKETT (1986) noted previously that most model pre-alteration Allende inclusions have superchondritic CaO/Al_2O_3 ratios and suggested that precursors of those inclusions condensed from a solar gas after ~20% of the Al was removed as corundum (Al_2O_3), the first major phase to condense from a cooling solar gas (GROSSMAN, 1972). Inclusions with superchondritic CaO/Al_2O_3 and TiO_2/Al_2O_3 ratios could have accumulated from such condensate precursors; however, removal of corundum alone cannot explain the origin of inclusions with superchondritic CaO/Al_2O_3 and subchondritic TiO_2/Al_2O_3 ratios. Those inclusions must have accumulated from precursors which condensed after a phase (or phases) with a subchondritic CaO/Al_2O_3 ratio and a superchondritic TiO_2/Al_2O_3 ratio, such as hibonite ($CaAl_{12}O_{19} \cdot CaMgTiAl_{10}O_{19}$), was removed from the gas. In four Allende FTAs studied by BECKETT (1986), hibonite has a mean CaO/Al_2O_3 ratio of 0.132 ± 0.001 × C1 chondrites and a mean TiO_2/Al_2O_3 ratio of 1.40 ± 0.11 × C1 chondrites. Hibonite forms by reaction of corundum with a solar gas at very high temperatures, 1727 K at 10^{-3} atm (HINTON et al., 1988).

BECKETT (1986) found that model pre-alteration Allende inclusions have higher SiO_2 and lower MgO concentrations than do model equilibrium solar condensates, as KERRIDGE (1981) observed using compositions of inclusions from various C3V chondrites, including altered Allende inclusions. BECKETT (1986) showed, however, that compositions of calculated condensate assemblages in a system containing 80% of the solar Al abundance have SiO_2 and MgO concentrations which closely match those of many pre-alteration Type A Allende inclusions. STOLPER (1982) suggested that the discrepancy between compositions of Type B inclusions and model condensates is due to the fact that calculations assume that the first-condensing clinopyroxene is diopside, rather than fassaite. As pointed out by GROSSMAN and CLARK (1973), fassaite is more likely, but insufficient thermodynamic data exist for this phase. According to STOLPER (1982) and BECKETT (1986), Type B inclusions formed by reaction

of Type As with the cooling nebular gas to form fassaite or by addition of fassaite to Type As.

Figure 4 is a plot of MgO vs. SiO_2 concentrations of inclusions from the reduced subgroup and of model pre-alteration Allende inclusions used to compile Table 3. Also shown are trajectories of model condensates at a total pressure of 10^{-3} atm, calculated as in LATTIMER and GROSSMAN (1978), but updated with newer thermodynamic data in ROBIE et al. (1978), ROBINSON et al. (1982), GEIGER et al. (1988), and CHAMBERLIN et al. (1991, and pers. commun.). The new results are similar to those of previous work except that, although diopside was a condensate in earlier work, no clinopyroxene appears in the latest calculations. The solid line labelled "no fass" in Fig. 4 is the resulting trajectory of equilibrium condensates from a solar gas. Another such trajectory, the solid line labelled "fass + sp" in Fig. 4, was calculated for the bulk condensate assemblage, assuming that fassaitic clinopyroxene condenses at 1450 K, slightly higher than the diopside condensation temperature of LATTIMER and GROSSMAN (1978), that the fassaite forms by complete reaction with the gas of the previously condensed melilite and perovskite, and that the fassaite contains equal moles of TiO_2 and Ti_2O_3 and the average Al_2O_3 content, 15.1%, of Allende fassaite having the same Ti content as is produced by these assumptions. The dashed lines trace the paths of model condensate compositions calculated in an identical manner to those represented by the solid lines but at 80% of the solar abundance of Al.

Figure 4 indicates that compositions of almost all inclusions from the reduced subgroup, like model Allende inclusions, tend to have higher SiO_2 and/or lower MgO concentrations than do equilibrium condensate assemblages from a solar gas whose compositions are calculated assuming that fassaite is not a condensate, although three Type As and two Type Bs

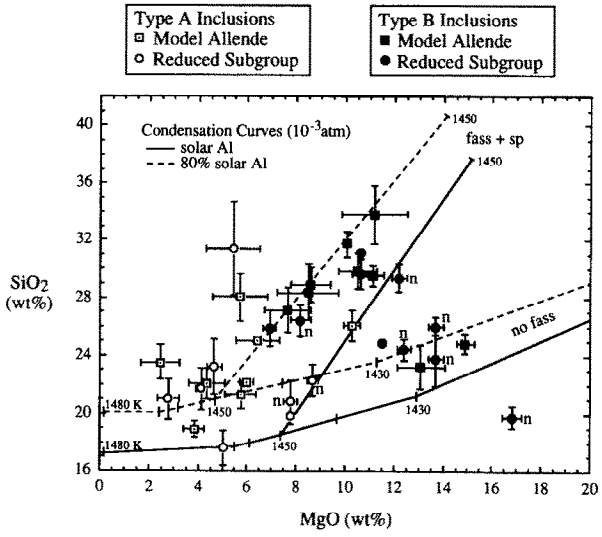

FIG. 4. SiO_2 vs. MgO concentrations of model Allende and reduced subgroup Type As and Bs, and of calculated condensate assemblages (see text). 1σ error bars shown on inclusion compositions where larger than plotted symbols. Data points for possibly nonrepresentative samples marked by "n". Numbers on condensate trajectories are condensation temperatures, and tick marks are plotted at 10° temperature intervals.

plot close to this condensation trajectory above and below 1450 K, respectively. When fassaite condensation is included, only a few more Type As and Bs plot along the trajectory. The trajectory would pass through many more of the Type B compositions if fassaite were stable enough to condense at $T > 1470$ K. In both cases, however, a cluster of high-MgO, low-SiO_2 Type Bs are clearly bypassed. While it is possible that physicochemical conditions allowed fassaite condensation in some parts of the solar nebula but prevented it elsewhere, we do note that a relatively large proportion (4/7) of the high-MgO, low-SiO_2 Type Bs may have been sampled nonrepresentatively. The effect of prior removal of 20% of the Al_2O_3 is seen in the condensation trajectory for a system with 80% of the solar abundance of Al. As found by BECKETT (1986), a large proportion of the Type As fall along this curve above 1450 K, but most Type Bs still have higher SiO_2 and/or lower MgO contents than condensates formed in this way, assuming that fassaite is not a condensate. As predicted by STOLPER (1982) and BECKETT (1986), however, the low-Al_2O_3 condensation trajectory passes right through the compositions of most Type Bs when the effect of the possible condensation of fassaite is taken into account.

REFRACTORY TRACE ELEMENTS

Enrichment factors relative to C1 chondrites for refractory trace elements in Vigarano, Leoville, and Efremovka inclusions are plotted in Figs. 5, 6, and 7, respectively. In the figures, the rare earth elements (REEs) are plotted from left to right in order of decreasing ionic radius. Other refractory lithophile elements (Zr, Hf, Sc, Th, Ta, V, Sr, Ba) and refractory siderophile elements (W, Re, Os, Ir, Mo, Ru) are plotted in order of increasing volatility in a solar gas, as summarized by SYLVESTER et al. (1992). C1 chondrite-normalization factors used in these figures and throughout this paper are from ANDERS and GREVESSE (1989) and are listed in Table 2.

Refractory Lithophiles in Inclusions with Group I REE Patterns

Group I REE patterns are those in which no REE except Eu is fractionated beyond analytical uncertainty from any other REE relative to C1 chondrites. In inclusions with such REE patterns, refractory lithophiles other than REEs may also be unfractionated from one another and from the REEs. More commonly, some refractory lithophiles are fractionated from others relative to C1 chondrites in individual Allende inclusions with Group I REE patterns. These fractionations are usually <20%, but larger fractionations do occur. For example, according to the summary of SYLVESTER et al. (1992), some inclusions have Eu anomalies of up to a factor of two. Also, ratios of abundances of refractory lithophiles other than REEs to those of REEs with similar volatility (such as Hf/Lu, Sc/Lu, Zr/Lu, Th/La, Ta/La, V/Yb, Sr/Yb, Ba/Yb) sometimes differ from the ratios of the same elements in C1 chondrites by as much as a factor of 4.5. Some inclusions even have significantly fractionated, so-called modified Group I REE patterns, in which REE enrichment factors vary progressively with atomic number. Nevertheless, despite the sometimes large fractionations among refractory

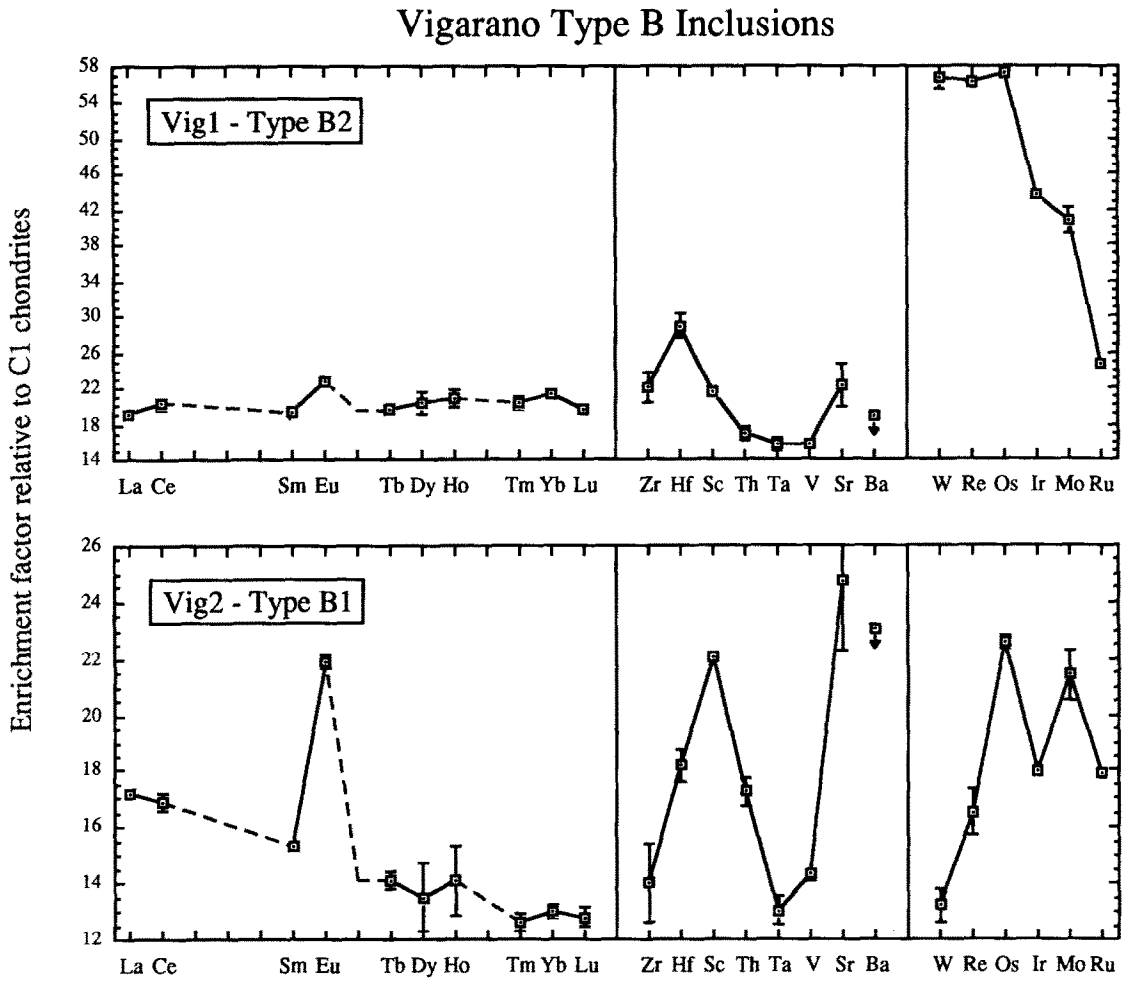

FIG. 5. C1 chondrite-normalized concentrations of REEs, other refractory lithophiles, and refractory siderophiles in Vigarano inclusions. Refractory lithophiles and siderophiles are arranged in order of increasing volatility from left to right. 1σ error bars shown where larger than plotted symbols. Arrows indicate 2σ upper limits. (a) Vig1; (b) Vig2.

lithophiles in individual Allende Group I inclusions, GROSSMAN and GANAPATHY (1976a) and GROSSMAN et al. (1977) showed that fractionations among these elements are always much smaller when averages of their concentrations in suites containing as few as nine inclusions are considered. This is thought to imply that precursors of refractory inclusions with Group I REE patterns were isolated from the nebular gas at temperatures low enough that each refractory lithophile element was fully condensed into them. In the average Allende Group I inclusion, refractory lithophile element concentrations are ~18 times C1 chondrites, suggesting that their precursors formed from the most refractory 5.6% of chondritic matter.

Large fractionations among refractory lithophile elements in individual inclusions with Group I and modified Group I REE patterns may reflect nonrepresentative nebular sampling from this overall unfractionated assemblage of condensate phases, which have strong crystal-chemical preferences for one refractory lithophile element relative to another. Activity coefficients required to take these effects into account when calculating the distribution of refractory lithophiles among possible condensate phases are unknown, but it has been inferred that hibonite, perovskite, and zirconium oxide were the major hosts for Sc, Th, Zr, Ta, Hf, and REEs other than Eu (DAVIS et al., 1978; FAHEY et al., 1987; HINTON et al., 1988; IRELAND et al., 1988), whereas melilite was the major host for Eu and Sr (GROSSMAN et al., 1977). Hibonite, perovskite, and melilite are thought to have preferred light REEs (LREEs) to heavy REEs (HREEs) during condensation, whereas zirconium oxide probably preferred HREEs over LREEs. Another possible explanation for large fractionations among refractory elements in such inclusions is laboratory sampling in such a way that the material selected from an inclusion is not representative of the whole. In the case of compact Type A and Type B inclusions, in which the original nebular phases were melted after accumulation into inclusion precursors, nonrepresentative laboratory sampling results in fractionations related to element redistribution caused by crystal-liquid partitioning rather than condensation or evaporation processes.

Vig1, Ef3, L2

These inclusions have Group I REE patterns. In Vig1's pattern (Fig. 5a), enrichment factors are ~20 × C1 and there is a small positive Eu anomaly. In contrast to Allende

Group I inclusions, which have Hf/Lu ratios of ~0.40–1.1 × C1 (SYLVESTER et al., 1992), the Hf/Lu ratio of Vig1 is ~1.5 × C1. Thus, the precursor phase or phases that carried much of the Hf into Vig1 probably had a strong crystal-chemical preference for Hf relative to Lu. Of zirconium oxide, perovskite, and hibonite, thought to be the major condensate hosts for Hf, there is evidence only for condensate hibonite having Hf/Lu ratios as high as 1.5 × C1. In inclusion 1105-42 from the Ornans C3O chondrite, zirconium oxide that possesses an ultrarefractory REE pattern and thus almost certainly had a condensate origin (DAVIS, 1991) has Hf/Lu ratios of 0.89–1.2 × C1 (A. Davis, pers. commun.). In the Murchison C2M chondrite, IRELAND et al. (1988) found that three perovskite and thirty-two hibonite grains which may be nebular condensates have mean Hf/Lu ratios of 0.17 ± 0.02 and 3.1 ± 0.7 × C1, respectively. Preferential sampling of hibonite alone probably cannot explain the superchondritic Hf/Lu ratio of Vig1, however, because, while the Zr/Lu and Sc/Lu ratios of Vig1 are only marginally superchondritic (~1.1 × C1), the hibonites of IRELAND et al. (1988) have mean Zr/Lu and Sc/Lu ratios of 3.9 ± 0.9 and 5.1 ± 1.0 × C1, respectively.

The Group I REE pattern of Ef3 (Fig. 7c), like that of Vig1, has a positive Eu anomaly. Enrichment factors for REEs except Eu are ~16 × C1. Ef3 is unusual compared to Allende Group I inclusions in that sizes of fractionations between Lu and Zr (Zr/Lu ~2.8 × C1), Hf (Hf/Lu ~2.6 × C1) and Sc (Sc/Lu ~ 3.1 × C1) equal or exceed the largest of those in Allende Group I CAIs (Zr/Lu ~0.54–1.1 × C1, Hf/Lu ~0.40–1.1 × C1, Sc/Lu ~0.66–2.7 × C1; SYLVESTER et al., 1992). Also, the V/Yb ratio of Ef3 is superchondritic (~1.5 × C1), while Allende Group I CAIs have subchondritic to chondritic V/Yb ratios (~0.22–0.99 × C1; SYLVESTER et al., 1992). The anomalously high Zr/Lu, Hf/Lu, Sc/Lu, and V/Yb ratios of Ef3 cannot be related to the fact, noted earlier, that our INAA sample is poorer in fassaite than the corresponding thin section. This is because the flat REE pattern and positive Eu anomaly of Ef3 are strong evidence that the sample taken for INAA was more representative of the whole inclusion than was the thin section. When fassaite and melilite cocrystallize from a melt, fassaite is substantially enriched in HREEs and depleted in Eu compared to melilite. If the bulk composition of Ef3 were actually enriched in HREEs, it would be most fortuitous if we had undersampled fassaite relative to melilite by just the right amount to result in a flat REE pattern.

Preferential nebular sampling of hibonite and/or zirconium oxide, either condensates or evaporative residues, has probably led to the anomalous Zr/Lu, Hf/Lu, Sc/Lu, and V/Yb ratios of Ef3. The probable crystal-chemical preference of hibonite for Zr, Hf, and Sc over Lu was discussed in the preceding text, using compositions of Murchison hibonite grains from IRELAND et al. (1988). Many of those same grains have superchondritic V/Yb ratios, the highest being ~11 × C1. In the zirconium oxide in Ornans 1105-42 (DAVIS, 1991), Sc/Lu and Zr/Lu ratios are only 0.02–0.07 and 0.68–1.1 × C1, respectively (A. Davis, pers. commun.). HINTON et al. (1988), however, found that, in a corundum-hibonite inclusion (BB-5) from Murchison, a trace phase, probably zirconium oxide and thought to be a nebular condensate, has Sc/Lu and Zr/Lu ratios of ~4.4 and ~18 × C1, respectively. The Hf/Lu and V/Yb ratios of this phase were not measured.

In L2, enrichment factors for REEs (Fig. 6b) are ~22–24 × C1 and there is no Eu anomaly. The CAI has strongly subchondritic V/Yb (~0.53 × C1) and Zr/Hf (~0.41 × C1) ratios, as do many Allende Group I inclusions, but is unusual in that Hf is fractionated from Zr to a degree that has yet to be seen in Allende Group Is (Zr/Hf ~0.76–1.5 × C1; SYLVESTER et al., 1992). The condensate or residue phases that carried much of the Hf and Yb into L2 apparently had subchondritic Zr/Hf and V/Yb ratios, which seems to rule out hibonite and perovskite. In Murchison, the thirty-two hibonite grains of IRELAND et al. (1988) that may be condensates have a mean Zr/Hf ratio of 1.5 ± 0.1 × C1 and, as noted, many of those same grains have superchondritic V/Yb ratios. Three Murchison perovskite grains analyzed by IRELAND et al. (1988) have strongly subchondritic V/Yb ratios (≤0.08 × C1), but strongly superchondritic Zr/Hf ratios (≥2.9 × C1). Zirconium oxide is a possible carrier of substantial amounts of Hf and Yb into L2, but the Zr/Hf ratios of the probable condensate grains of this phase in Ornans (0.76–0.95 × C1, A. Davis, pers. commun.) are not as low as that in L2.

L1, Ef2, Vig2, Ef1, L5

These inclusions have modified Group I REE patterns. There is no evidence from comparisons of observed and calculated modes (Table 1) that any of the five, except perhaps Vig2, is a nonrepresentative sample of the bulk inclusion from which it was derived.

Two of the five inclusions, L1 and Ef2, have refractory lithophile element characteristics that are rare or absent in Allende inclusions. In L1, C1 chondrite-normalized enrichment factors (Fig. 6a) for LREEs (~20–22) are smaller than those for HREEs (~25–29), there is a small positive Eu anomaly, and Zr/Lu (~1.2 × C1), Hf/Lu (~1.7 × C1), and Sc/Lu (~1.5 × C1) ratios are superchondritic. What makes L1 unusual compared to Allende Group I inclusions is its extremely low V/Yb ratio, 0.25 ± 0.01 × C1. Subchondritic V/Yb ratios, as noted, may reflect preferential sampling of perovskite relative to other condensate or residue phases in the nebula. Because the Murchison perovskites of IRELAND et al. (1988) have chondritic Sc/Lu ratios and subchondritic Zr/Lu and Hf/Lu ratios, however, L1 must have preferentially sampled not only perovskite precursors, but also another phase such as the zirconium oxide of HINTON et al. (1988). That phase, like L1, has smaller C1 chondrite-normalized enrichment factors for LREEs than for HREEs and, as noted, superchondritic Sc/Lu and Zr/Lu ratios.

In the REE pattern of Ef2 (Fig. 7b), enrichments decrease slightly from La (~14 × C1) to Sm (~12 × C1), increase slightly from Tb (~12 × C1) to Yb (~14 × C1), and there is a very large positive Eu anomaly. What makes Ef2 unusual compared to Allende inclusions is its high Eu/Sm (~2.2 × C1), Sr/Yb (~2.4 × C1), and Th/La (~1.6 × C1) ratios and, like L1, described in the preceding text, its low V/Yb (0.25 ± 0.01 × C1) ratio. The unusually large Eu/Sm and Sr/Yb ratios in Ef2 probably reflect sampling of melilite in

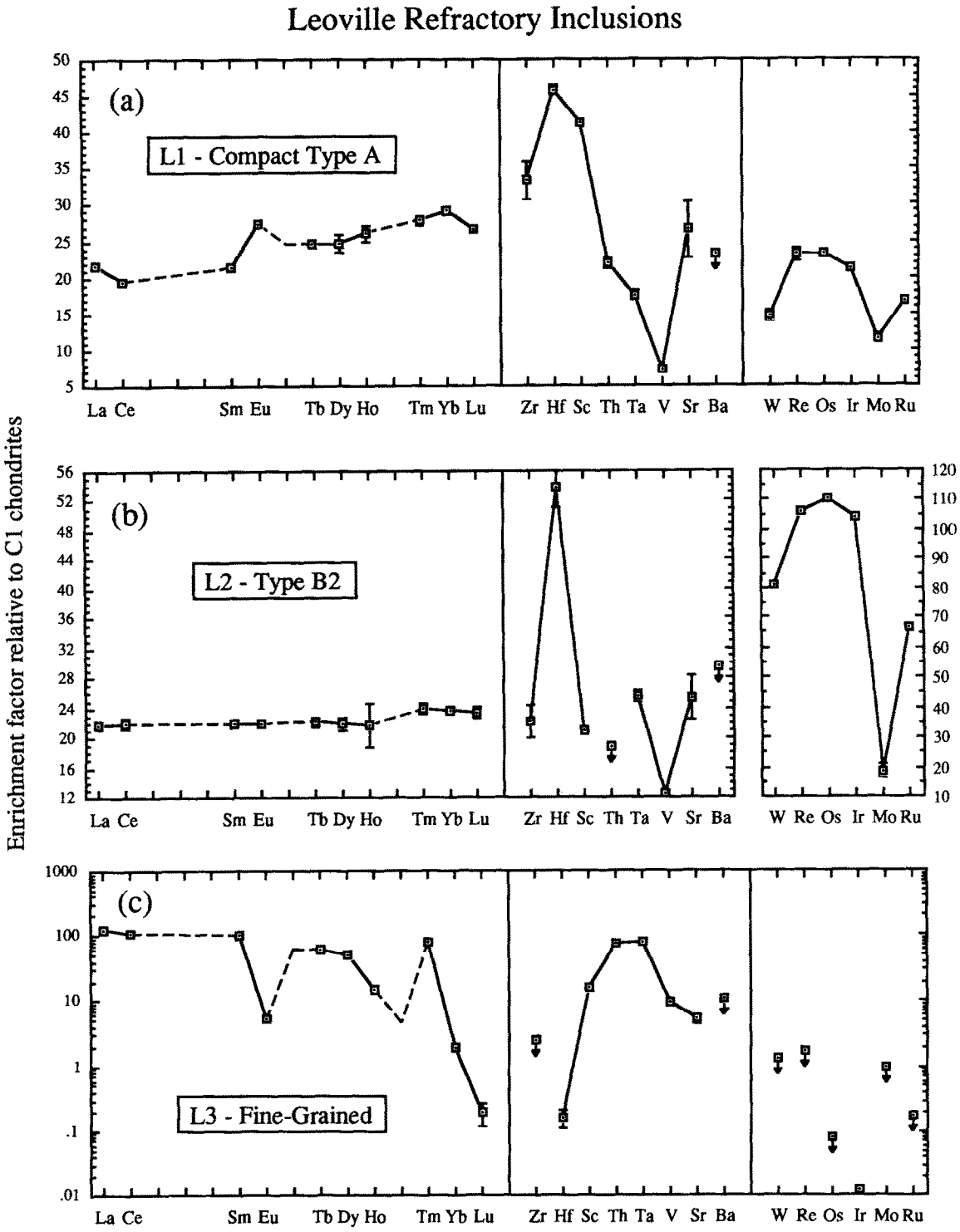

FIG. 6. C1 chondrite-normalized concentrations of REEs, other refractory lithophiles, and refractory siderophiles in Leoville inclusions. Refractory lithophiles and siderophiles are arranged in order of increasing volatility from left to right. 1σ error bars shown where larger than plotted symbols. Arrows indicate 2σ upper limits. (a) L1; (b) L2; (c) L3 (note logarithmic scale); (d) L4; (e) L5.

preference to other condensate or residue phases in the nebula, because melilite is thought to carry the bulk of the Eu and Sr, but not the bulk of the Sm and Yb, into refractory inclusions (GROSSMAN et al., 1977). The large Th/La ratio of Ef2 is consistent with the suggestion of SYLVESTER et al. (1992) that the bulk of the Th was carried into inclusions by a condensate or residue phase that did not contain the bulk of the REEs. SYLVESTER et al. (1992) found two Vigarano inclusions with strongly subchondritic Th/La ratios, suggesting that the Th carrier phase was undersampled in the

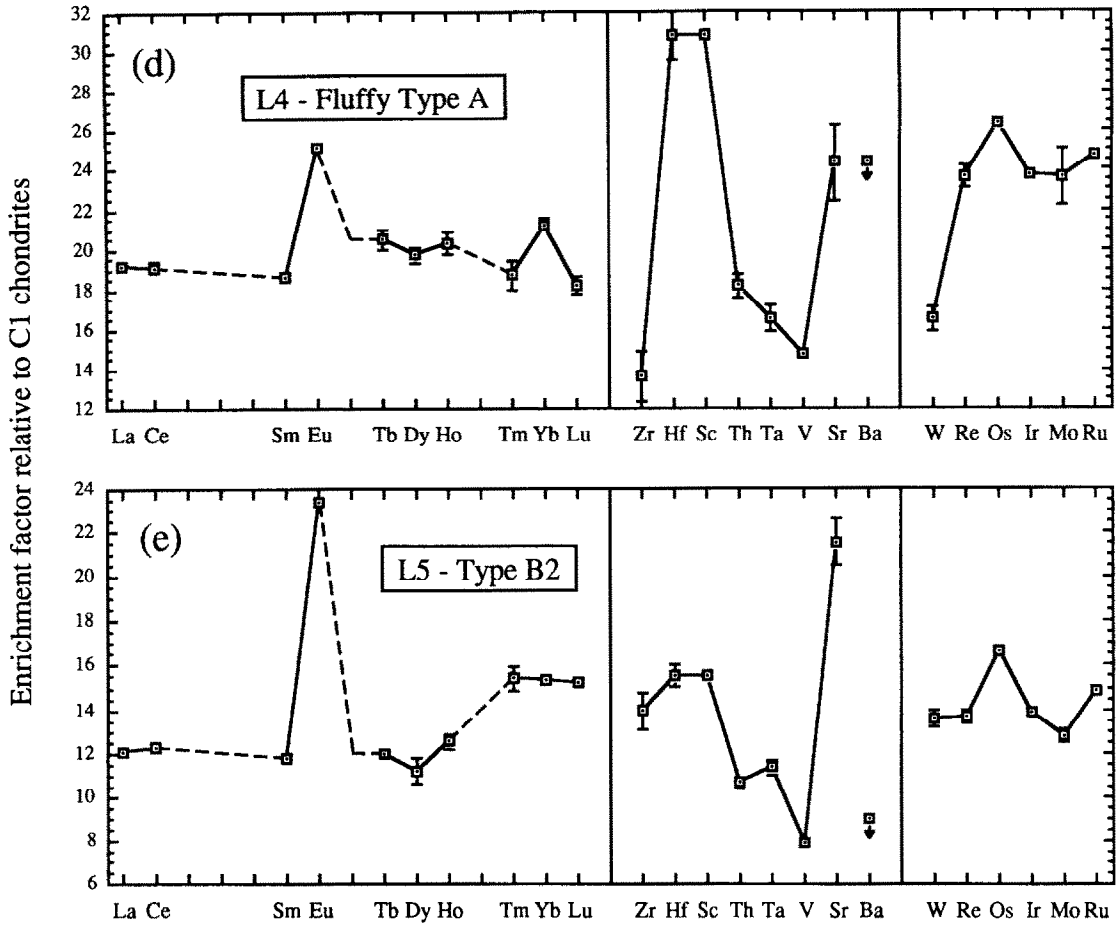

FIG. 6. (Continued)

nebula, whereas in Ef2, that phase seems to have been oversampled.

Vig2 (Fig. 5b) and Ef1 (Fig. 7a) have LREE-enriched chondrite-normalized REE patterns, with positive Eu anomalies. In Vig2, REE enrichment factors decrease slightly from ~17 × C1 for La and Ce to ~13–14 × C1 for the HREEs. In Ef1, REE enrichment factors decrease slightly from ~19 × C1 for La and Ce to ~16–17 × C1 for HREEs. In both inclusions, Zr, Hf, Sc, Th, Ta, V, and Sr are each fractionated from a REE of similar volatility by less than a factor of 2, relative to C1 chondrites. The Sc/Lu (~1.7 × C1) and Hf/Lu (~1.4 × C1) ratios of Vig2 are particularly large. Sr/Yb ratios of both Vig2 (~1.9 × C1) and Ef1 (~1.6 × C1) are also large, but still smaller than that of Ef2.

For Ef1, the positive Eu anomaly, LREE enrichment and high Sr/Yb ratio may all be due to preferential nebular sampling of melilite relative to other condensate or residue phases. For Vig2, however, Table 1 indicates that our INAA sample has more melilite and less fassaite than its corresponding thin section. Because melilite prefers LREEs over HREEs (KUEHNER et al., 1989) and fassaite prefers HREEs over LREEs (SIMON et al., 1991) relative to C1 chondrites in melts having the compositions of Type B inclusions, it is possible that the mode of our thin section accurately represents that of the whole of Vig2 and that the latter actually has a flat REE pattern. While this would explain the LREE enrichment, positive Eu anomaly, and high Sr/Yb ratio of our sample of Vig2, it would also imply that the Sc/Lu and Hf/Lu ratios of the whole of Vig2 are even higher than those measured because fassaite prefers Sc and Hf over Lu during crystallization of melts of these compositions (SIMON et al., 1991). Enhancement of these ratios may be due to sampling of unusually large amounts of condensate or residue hibonite amongst the precursors of Vig2.

L5 (Fig. 6e) has a REE pattern in which Tm, Yb, and Lu (~15 × C1) are slightly enriched relative to La, Ce, Sm, Tb, Dy, and Ho (~12 × C1), and Eu and Sr have large enrichment factors (~22 × C1). Vigarano 1623-11, an inclusion analyzed by SYLVESTER et al. (1992), has similar characteristics which were explained in terms of preferential nebular sampling of condensate melilite, carrying the bulk of the Eu and Sr, and of zirconium oxide, carrying the bulk of the HREEs, relative to perovskite, carrying the bulk of the LREEs. This may also be the case for L5. In addition, Zr, Hf, and Sc, which have enrichment factors like those of Tm, Yb, and Lu in L5, may have been largely concentrated in zirconium oxide, while Th and Ta, which are enriched to about the same degree as La, Ce, Sm, Tb, Dy, and Ho, may have been largely in perovskite. Enrichment factors for V (~8 × C1) and Ba (<9 × C1) are smaller than those of all other refractory lithophiles in L5. GROSSMAN et al. (1977) inferred that Ba was carried into Allende inclusions by an unknown phase

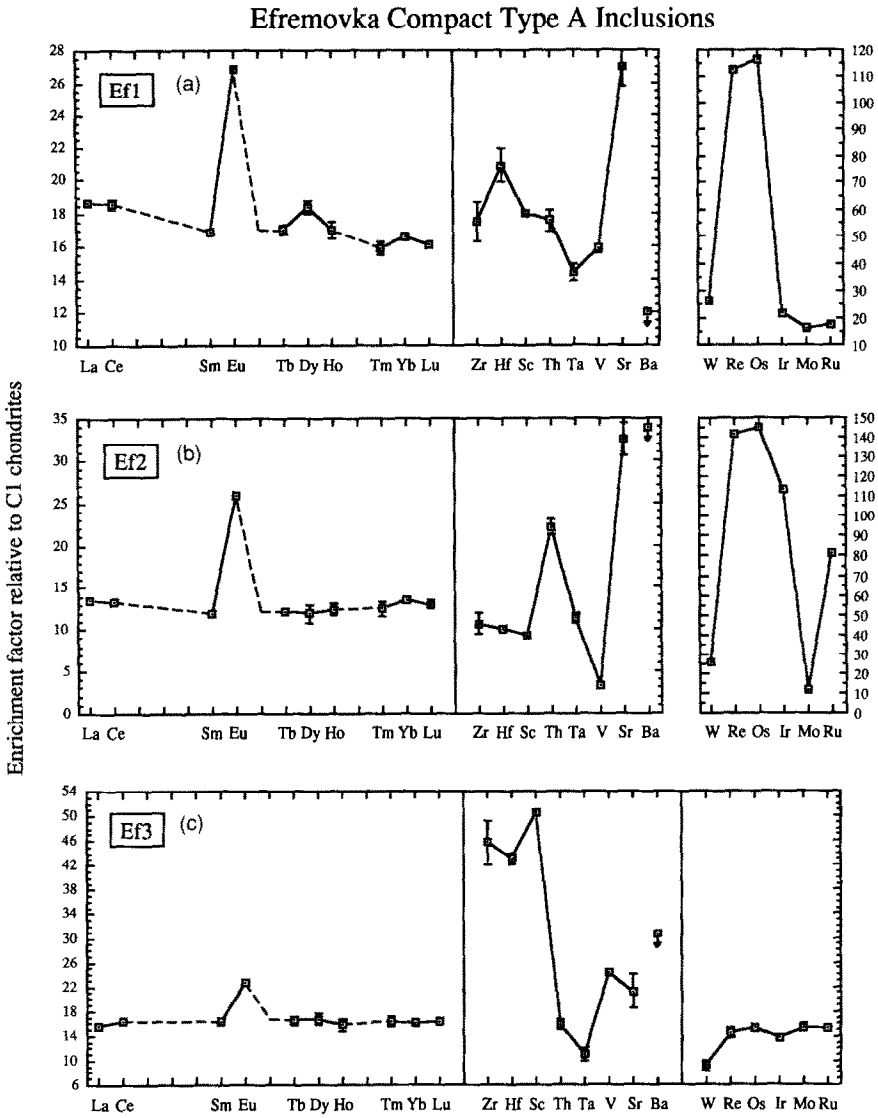

FIG. 7. C1 chondrite-normalized concentrations of REEs, other refractory lithophiles, and refractory siderophiles in Efremovka inclusions. Refractory lithophiles and siderophiles are arranged in order of increasing volatility from left to right. 1σ error bars shown where larger than plotted symbols. Arrows indicate 2σ upper limits. (a) Ef1; (b) Ef2; (c) Ef3.

that did not possess significant amounts of other refractory lithophiles. L5 may have undersampled that Ba-rich phase.

Refractory Siderophiles in Group I Inclusions

Six of the eight Group I inclusions studied here have unusual or unique refractory siderophile element compositions compared to most Allende Group I inclusions. In nine of the latter, mean C1 chondrite-normalized concentrations of each of Re, Os, Ir, and Ru are 16.2 ± 0.4 and, in each of the nine inclusions, these siderophiles are fractionated from one another by <20% (GROSSMAN et al., 1977). Enrichment factors for Re, Os, Ir, and Ru are similarly unfractionated in L5 and Ef3, mean concentrations being $\sim 15 \times$ C1 in each.

L1 is unusual in that Ru has an enrichment factor relative to C1 chondrites (~ 17) that is less than those of Re and Os by 28% and of Ir by 21%. Vig2 is unusual in that the enrichment factor of Os ($\sim 23 \times$ C1) is greater than those of Re (by 37%) and Ir and Ru (by 26%). This enrichment pattern is similar to that of Vig 1623-3, a Vigarano inclusion analyzed by MAO et al. (1990), in which concentrations of Re, Ir, and Ru are $\sim 11 \times$ C1, while that of Os is $\sim 27 \times$ C1.

Some of the refractory siderophile element enrichment factors, and fractionations between those siderophiles, in the four other Group I inclusions of this study, Vig1, L2, Ef1, and Ef2, are the largest ever discovered in bulk CAIs. In Vig1, enrichment factors relative to C1 chondrites decrease from Re and Os (~ 57), which are most refractory, to those for Ir (~ 44) and Ru (~ 25), which are progressively less refractory. In L2, Re, Os, and Ir are uniformly enriched to $\sim 110 \times$ C1, whereas Ru is $\sim 66 \times$ C1. In Ef1, Re and Os are $\sim 115 \times$ C1 and Ir and Ru are ~ 22 and $17 \times$ C1, respectively. In Ef2, Re and Os are $\sim 145 \times$ C1, Ir is $\sim 114 \times$ C1, and Ru is $\sim 81 \times$ C1. Although refractory siderophile element enrichment factors as large as those found here have not been reported previously for bulk CAIs, NAZAROV et al.

(1987) described two Efremovka inclusions that contain very abundant, large grains of refractory siderophile element-rich FeNi metal. Those two inclusions, like Ef1 and Ef2 reported here, presumably have bulk compositions with large refractory siderophile enrichment factors. The present work extends the observation of very high refractory siderophile enrichment factors to CAIs in two other members of the reduced subgroup, Vigarano and Leoville.

In individual Allende Group I inclusions, C1 chondrite-normalized concentrations of W and Mo are equal to or less than those of Re, Os, Ir, and Ru (GROSSMAN et al., 1977; FEGLEY and PALME, 1985). Those with subchondritic W/Re and Mo/Ir ratios are said to possess negative W and Mo anomalies, respectively. Of the eight Group I inclusions of this study, L5 and Vig1 have nearly chondritic W/Re and Mo/Ir ratios. Vig2 and Ef3 have negative W anomalies but Mo/Ir ratios of $\sim 1.2 \times$ C1 and $\sim 1.1 \times$ C1, respectively. L1, L2, Ef1, and Ef2 have both negative W and negative Mo anomalies. In L1, W/Re and Mo/Ir ratios are both $\sim 0.6 \times$ C1. Negative Mo anomalies are larger than negative W anomalies in L2 and Ef2, but in Ef1 the reverse is true.

Refractory siderophiles are thought to have been carried into refractory inclusions by metal-alloy condensate phases. SYLVESTER et al. (1990) proposed that W and Mo, whose high-temperature crystal structures are body-centered cubic (bcc), condensed into one alloy phase; Re, Os, and Ru, which are hexagonal close-packed (hcp), condensed into a second alloy phase; and Ir, Pt, and Rh, which are face-centered cubic (fcc), condensed into a third alloy phase. If an alloy is removed from the nebular gas at a temperature above that at which its constituent refractory siderophiles have fully condensed, depletions of the more volatile siderophiles relative to the less volatile ones will result, relative to C1 chondrites. SYLVESTER et al. (1990) inferred that such fractionated alloys accreted into precursors of Allende inclusions because, in one such inclusion, metal-alloy assemblages (Fremdlinge) have large fractionations of refractory siderophiles from one another. Thus, in inclusions with nearly chondritic ratios of Re, Os, Ru, and Ir, such as L5, Ef3, and most Allende Group I inclusions, large numbers of hcp and fcc alloy grains must have been sampled so that fractionations between refractory siderophiles of the two different alloys, and those between siderophiles of the same alloy, were averaged out. This apparently was not the case for the six unusual Group I inclusions studied here, L1, L2, Vig1, Vig2, Ef1, and Ef2.

In Vig1, Ef1, and Ef2, C1 chondrite-normalized enrichment factors for Ir are significantly lower than those for Re and Os. Either Ir was incompletely condensed into the fcc alloy grains sampled by those inclusions or, relative to their nebular proportions, those fcc grains were undersampled compared to hcp grains. In L1, L2, Vig1, Ef1, and Ef2, enrichment factors for Ru are significantly lower than those for Re and Os, which are present in nearly chondritic ratios. Precursors of these inclusions probably oversampled hcp grains with chondritic Re/Os and superchondritic Os/Ru ratios. At a pressure of 10^{-3} atm, hcp alloys removed from a solar gas below ~ 1750 K, where Re and Os are fully condensed, and above ~ 1490 K, where Ru is fully condensed, will have chondritic Re/Os and superchondritic Os/Ru ratios. Removal temperatures for the mean compositions of model hcp alloys in L1, L2, Vig1, Ef1, and Ef2 range from ~ 1655 K for Ef1 to ~ 1590 K for L1.

The remarkably large enrichment factors for Re and Os in L2, Vig1, Ef1, and Ef2 relative to those in typical Allende Group I inclusions imply that the total amount of hcp alloy accreted by L2, Vig1, Ef1, and Ef2 is 3.5–9.1 times that accreted by those Allende inclusions. It may seem curious that Re, Os, and Ru are averaged out to their chondritic proportions in Allende inclusions even though they sampled less hcp alloy than did L2, Vig1, Ef1, and Ef2, in which Ru is so strongly depleted relative to Re and Os. The latter inclusions, however, as well as the millimeter-sized metal nugget with Ru/Re $\sim 0.3 \times$ C1 reported by NAZAROV et al. (1987) from an Efremovka inclusion, sampled hcp alloys which, on average, were removed from the nebular gas at temperatures above which Ru fully condenses, whereas Allende inclusions sampled hcp alloys with lower mean equilibration temperatures.

Vig2 has subchondritic Re/Os and superchondritic Os/Ru ratios. Because Re is more refractory than Os, hcp alloy grains with subchondritic Re/Os ratios can condense from a cooling solar gas only if high-temperature hcp alloy grains with superchondritic Re/Os ratios were removed from that gas previously. Single-stage removal of hcp alloy grains at 1840 K yields a subsequently condensing hcp alloy at 1630 K with the Re/Os and Os/Ru ratios of Vig2.

Negative W and Mo anomalies in L1, L2, Ef1, and Ef2 probably reflect undersampling of bcc relative to hcp and fcc condensate alloy grains in the nebula. Negative W anomalies without accompanying negative Mo anomalies in Vig2 and Ef3 may be the result of preferential nebular sampling of bcc condensate alloy grains with subchondritic W/Mo ratios. Such grains can condense after removal of early, high-temperature bcc alloys which, because W is more refractory than Mo in a solar gas (e.g., SYLVESTER et al., 1990), have superchondritic W/Mo ratios. An alternative model for W and Mo depletions in bulk inclusions is condensation from an oxidizing gas (FEGLEY and PALME, 1985). Because Mo is more volatile than W in an oxidizing gas, negative Mo anomalies should be larger than negative W anomalies in condensates from such a gas, which is the case for L2 and Ef2, but not for L1, Ef1, Vig2, and Ef3.

Inclusion with a Group II REE Pattern

L3, the only fine-grained inclusion of this study, has a Group II REE pattern (Fig. 6c) like most Allende fine-grained inclusions. REEs with the largest enrichment factors are La ($\sim 123 \times$ C1), Ce ($\sim 107 \times$ C1), Sm ($\sim 104 \times$ C1), and Tm ($\sim 81 \times$ C1). Enrichment factors for other HREEs progressively decrease with increasing atomic number from Tb ($\sim 62 \times$ C1) to Lu ($\sim 0.2 \times$ C1), and enrichment factors for Eu ($\sim 6 \times$ C1) and Yb ($\sim 2 \times$ C1) are anomalously small. In L3, as in Allende Group IIs, the most refractory (Zr, Hf, Sc) and most volatile (V, Yb, Eu, Sr, Ba) of the refractory lithophiles, and the refractory siderophiles, have lower enrichment factors than those of refractory lithophiles of intermediate volatility (Th, Tm, La, Ce, Sm, Ta). This strongly suggests that the precursor phases of L3, like those of Allende Group IIs, condensed from the nebular gas after

removal of an early, ultrarefractory condensate containing the most refractory of the lithophiles (BOYNTON, 1975; DAVIS and GROSSMAN, 1979) and the refractory siderophiles. Those precursors were then isolated from that gas before the most volatile of the refractory lithophiles could completely condense into them.

Inclusion with a Group VI REE Pattern

C1 chondrite-normalized Group VI REE patterns are those in which no REE is significantly fractionated from any other REE, except for Eu and Yb, which exhibit positive anomalies (MASON and TAYLOR, 1982). Inclusions with such patterns probably sampled two nebular components, one of which had a Group I REE pattern. The other condensed from the nebular gas at low temperatures, after high-temperature removal from that gas of each of the REEs, except for the most volatile ones, Eu and Yb.

L4 (Fig. 6d) has a Group VI REE pattern with an Eu/Sm ratio of $\sim 1.4 \times$ C1 and a Yb/Lu ratio of $\sim 1.2 \times$ C1. Chemical compositions of only a small number of Allende Group VI inclusions have been reported, but in the one (NM3529yc) analyzed by CONARD (1976), the one (5171) by MASON and MARTIN (1977), and the two (3529-44, 3529-Y) by MASON and TAYLOR (1982), Eu/Sm and/or Eu/Gd ratios are ~ 1.2–$1.5 \times$ C1 and Yb/Er, Yb/Tm, and/or Yb/Lu ratios are ~ 1.3–$1.4 \times$ C1, as in L4.

In a solar gas, assuming ideal solid solution, Ta and V are about as volatile as Eu and Yb, and Sr slightly more so (DAVIS et al., 1982). The low temperature condensate component of a Group VI inclusion should thus contain large concentrations of Sr, Ta, and V, in addition to large concentrations of Eu and Yb. Thus, Group VI inclusions should have enrichment factors for Sr, Ta, and V that are larger than those for trivalent REEs and about as large as those for Eu and Yb, assuming that the Group I component contains chondritic proportions of Sr, Ta, V, and REEs. In L4, Sr/Eu and Sr/Yb ratios are nearly chondritic but Ta/La and V/La ratios are subchondritic, suggesting that enrichment factors for Ta and V in the Group I component of L4 are much smaller than those for REEs. Among Allende Group VI inclusions, sample NM3529yc of CONARD (1976) not only has subchondritic Ta/La and V/La ratios, but also subchondritic Sr/Eu and Sr/Yb ratios. Strontium may have condensed incompletely into the low-temperature component of NM3529yc. Sample 5171 of MASON and MARTIN (1977), in contrast, has a Sr/Eu ratio of $\sim 1.3 \times$ C1 and a Sr/Yb ratio of $\sim 1.1 \times$ C1, suggesting complete condensation of Sr into its low temperature precursors.

Because Zr, Hf, and Sc are among the most refractory lithophile elements, they are thought to have condensed, along with trivalent REEs, into the Group I component of Group VI inclusions. Among Allende Group VI inclusions, Hf and Sc are fractionated from Lu and/or Er by $\sim 35\%$ or less, relative to C1 chondrites, and Zr is fractionated from Hf by $\sim 17\%$ or less. L4 is therefore unusual in that Hf/Lu and Sc/Lu ratios are $\sim 1.7 \times$ C1 and the Zr/Hf ratio is $\sim 0.44 \times$ C1. As noted earlier for L2, subchondritic Zr/Hf ratios may be the result of preferential nebular sampling of zirconium oxide, although probable condensate grains of this phase have not been found with Zr/Hf ratios as low as this. Furthermore, those zirconium oxide grains that have been found with subchondritic Zr/Hf ratios also possess strongly subchondritic Sc/Lu ratios and nearly chondritic Hf/Lu ratios, in contrast to L4.

Refractory siderophiles in L4 have enrichment factors of ~ 24–$26 \times$ C1, except for W, which has a lower enrichment factor of ~ 17. The chondrite-normalized refractory siderophile element pattern of L4 is thus like that of many Allende Group I inclusions. Too little is known about the refractory siderophile element patterns of Allende Group VI inclusions to make comparisons with L4.

NONREFRACTORY ELEMENTS

Coarse-grained Inclusions

Nonrefractory elements, including Ni, Co, Mg, Fe, Si, Cr, Au, Mn, As, K, Na, Ga, Sb, Cl, Se, Cs, Zn, and Br, which were analyzed here, were probably added to refractory inclusions during low-temperature reaction with the nebular gas, producing secondary alteration products. Mg, Si, Cr, Ni, and Co are somewhat exceptional compared to other nonrefractory elements in that substantial fractions of the amounts present began condensing at high temperatures. Most coarse-grained inclusions of the reduced subgroup of C3V chondrites probably experienced secondary alteration at temperatures far above those at which many nonrefractory elements completely condensed from the nebular gas, or for a time that was far too short for many of those elements to be completely condensed in those inclusions. In contrast, most inclusions from the oxidized subgroup of C3V chondrites were probably altered at comparatively low temperatures or for longer times, although still not low or long enough for complete condensation. The evidence for this is from BISCHOFF et al. (1987), MAO et al. (1990), and SYLVESTER et al. (1992), who collectively found that coarse-grained inclusions from Arch, Efremovka, Leoville, and Vigarano, members of the reduced subgroup, possess Na and Au contents that fall below or within the lowermost parts of the ranges of concentrations of those elements in coarse-grained inclusions from Allende and Grosnaja, members of the oxidized subgroup. SYLVESTER et al. (1992) further showed that six coarse-grained refractory inclusions from Vigarano and Leoville tend to have lower Fe and Zn contents than do Allende inclusions, as compiled by DAVIS et al. (1982).

GROSSMAN and GANAPATHY (1976a) suggested that high concentrations of Fe, Co, and Mn seen in some Allende inclusions are due in part to contamination of those inclusions with meteoritic matrix material during laboratory sampling, but that the high concentrations of Cr, Au and Na in those inclusions are largely indigenous. In this study and those of MAO et al. (1990) and SYLVESTER et al. (1992), however, we were careful to avoid sampling near inclusion/matrix interfaces, so we believe that the concentrations of nonrefractory elements in inclusions of the reduced subgroup analyzed by us are indigenous.

In Figure 8a, Na and Au concentrations are plotted for each of the nine coarse-grained inclusions studied herein, and the inclusions considered previously by BISCHOFF et al. (1987), MAO et al. (1990), and SYLVESTER et al. (1992).

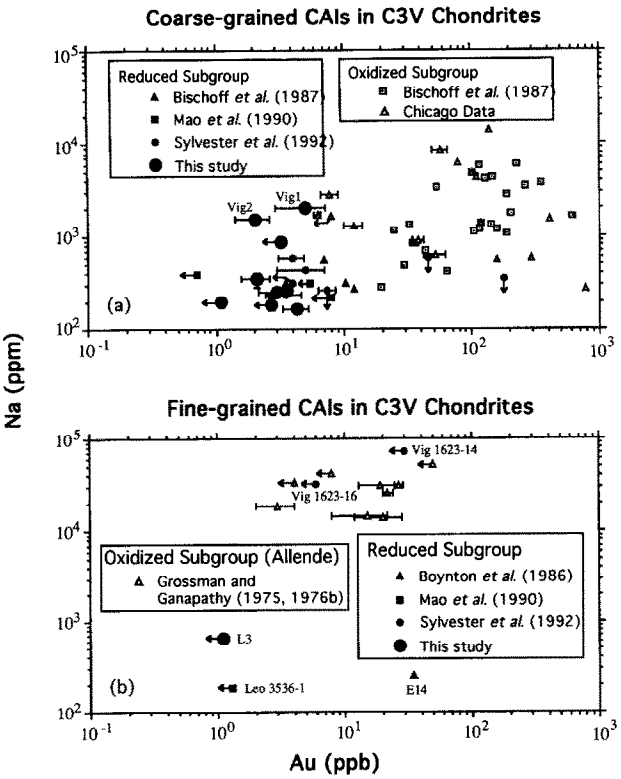

FIG. 8. Concentrations of Na and Au in (a) coarse-grained and (b) fine-grained CAIs of the oxidized and reduced subgroups of C3V chondrites. 1σ error bars shown where larger than plotted symbols. Arrows indicate 2σ upper limits.

Like coarse-grained inclusions of the reduced subgroup studied in previous work, the nine analyzed here have lower Au (<1.1–5.0 ppb) contents than those of the oxidized subgroup (6–800 ppb Au). Concentrations of Na in the nine inclusions of this study (170–860 ppm), except for Vig1 (2020 ppm) and Vig2 (1540 ppm), are lower than those of twenty-nine of thirty-seven inclusions of the oxidized subgroup. These observations are consistent with the paucity of secondary alteration products in the coarse-grained inclusions of this work, except Vig1, and support the idea that most coarse-grained inclusions of the reduced subgroup were altered in the nebular gas at a higher temperature or for a shorter time than most of those of the oxidized subgroup.

In Fig. 9, concentrations of Cr, Mn, Fe, Co, Ni, and Zn in the coarse-grained CAIs studied here are compared to those of coarse-grained Allende CAIs, as compiled by DAVIS et al. (1982). Concentrations of Cr, Mn, Fe, and Zn in most coarse-grained inclusions of this study fall below or within the lowermost parts of the ranges of concentrations of those elements in Allende coarse-grained inclusions. The low concentrations of Cr in the coarse-grained inclusions studied here contrast with generally higher concentrations of Cr (mean of 0.18 $\pm$ 0.03 $\times$ CI) seen in the six Vigarano and Leoville inclusions of SYLVESTER et al. (1992), so that Cr concentrations in coarse-grained inclusions of the reduced subgroup are not uniformly low and are, on average, comparable to those of Allende.

As in the six inclusions of SYLVESTER et al. (1992), the ranges of concentrations of Ni and Co in the coarse-grained inclusions of this study overlap with the corresponding ranges of Ni and Co contents in their Allende counterparts (Fig. 9). Even excluding two coarse-grained inclusions with anomalously high Ni and Co contents, Vig1 and Ef3, the remaining seven inclusions studied here have lower Ni concentrations than only nine of sixteen, and lower Co concentrations than only thirteen of thirty-two of the Allende inclusions of DAVIS et al. (1982). Thus, coarse-grained inclusions of both the reduced and oxidized subgroups may not have been removed from the nebular gas until significant amounts of Ni, Co, and Cr, which have the highest condensation temperatures of the nonrefractory elements considered here (e.g., PALME et al., 1988), condensed.

Fine-grained Inclusion

In Allende, fine-grained inclusions were more intensely altered by reaction with low-temperature nebular gas than their coarse-grained counterparts. Thus, for example, the mean concentrations of Na (2.9%), Mn (468 ppm), Fe (6.1%), and Zn (917 ppm) in nine fine-grained Allende inclusions analyzed by GROSSMAN and GANAPATHY (1975, 1976b) are greater than those for Na (2122 ppm), Mn (98 ppm), Fe (1.2%), and Zn (105 ppm) in ten coarse-grained Allende inclusions analyzed by GROSSMAN and GANAPATHY (1975, 1976a) and GROSSMAN et al. (1977).

In contrast, fine-grained inclusions of the reduced subgroup were altered under a variety of conditions such that some are more enriched in nonrefractory elements than are their coarse-grained counterparts, while others are not. Thus, the

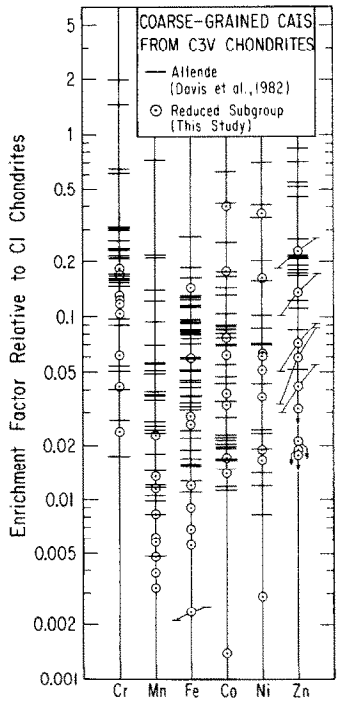

FIG. 9. Concentrations of Cr, Mn, Fe, Co, Ni, and Zn in coarse-grained CAIs of this study and from Allende, as compiled by DAVIS et al. (1982). For CAIs of this study, 1σ error bars are shown where larger than plotted symbols, and they are displaced from the vertical lines for clarity. Arrows indicate 2σ upper limits.

two fine-grained Vigarano inclusions of SYLVESTER et al. (1992) have concentrations of Na (3.17 and 7.14%), Mn (282 and 114 ppm), Fe (3.8 and 2.6%), and Zn (1320 and 1380 ppm) that are greater than the mean concentrations of Na (550 ppm), Mn (42 ppm), Fe (0.59%), and Zn (<28 ppm) in eighteen coarse-grained Vigarano, Leoville, and Efremovka inclusions analyzed by MAO et al. (1990), SYLVESTER et al. (1992), and in this study. Compared to the latter, however, the Leoville fine-grained inclusion of MAO et al. (1990) has lower concentrations of Na (185 ppm), Mn (31 ppm), Fe (0.25%), and Zn (<0.3 ppm), and the Efremovka fine-grained inclusion of BOYNTON et al. (1986) also has a lower concentration of Na (~250 ppm).

In Fig. 8b, a plot of Na vs. Au concentrations of fine-grained inclusions from the oxidized and reduced subgroups, the two Vigarano inclusions of SYLVESTER et al. (1992), Vig 1623-14, and Vig 1623-16, plot among Allende inclusions, while the Leoville inclusion of MAO et al. (1990), Leo 3536-1, has lower Na and Au contents than both Allende and Vigarano inclusions. The Efremovka inclusion of BOYNTON et al. (1986), E14, has a low Na concentration, like that of Leo 3536-1, and a high Au concentration, like those of the Vigarano and Allende inclusions. These results suggest that, while Leo 3536-1 was altered at a higher temperature or for a shorter time than were Allende fine-grained inclusions, Vig 1623-14 and Vig 1623-16 were altered under conditions similar to those experienced by Allende fine-grained inclusions. Because Na has a lower initial condensation temperature than Au in a solar gas (PALME et al., 1988), E14 was probably altered at a temperature above which Na is significantly condensed, but below which Au is significantly condensed.

The fine-grained Leoville inclusion of this study, L3, has concentrations of Na (641 ppm), Au (<1.1 ppb), Mn (21 ppm), Fe (0.33%), and Zn (<11 ppm) which are comparable to those in coarse-grained inclusions of the reduced subgroup. As shown in Fig. 8b, L3 is like Leo 3536-1 in that it has Na and Au contents that are lower than those of Allende and Vigarano fine-grained inclusions. Like Leo 3536-1, L3 probably experienced secondary alteration at a higher temperature or for a shorter time than Allende and Vigarano fine-grained inclusions.

CONCLUSIONS

Major element compositions of pristine CAIs from the reduced subgroup of C3V chondrites, like those of model Allende CAIs determined by BECKETT (1986), suggest that Type A inclusions formed from a different population of high-temperature nebular condensates than did Type B inclusions. Although many CTAs are distinct in major element composition from FTAs, some CTAs could be crystallization products of whole melts of FTAs. Nebular precursors which melted to form Type B1s had bulk compositions similar to those which melted to form Type B2s. All Type As and most Type Bs have superchondritic CaO/Al_2O_3 ratios, suggesting condensation of their nebular precursors after early removal of an Al-rich phase from a solar gas, as noted by BECKETT (1986). For inclusions with subchondritic TiO_2/Al_2O_3 ratios, mostly Type As, the early-removed phase may be hibonite, whereas for inclusions with superchondritic TiO_2/Al_2O_3 ratios, mostly Type Bs, that phase is probably corundum. High-temperature condensate precursor phases of most Type Bs seem to have reacted with the nebular gas to form fassaite at low temperatures and hence tend to possess larger concentrations of MgO and SiO_2 than Type As.

Refractory inclusions of the reduced subgroup are similar to their counterparts in Allende in that they have Groups I, II, and VI REE patterns and nearly chondritic ratios of many non-REE lithophiles to REEs with similar volatility. For instance, Sr/Eu ratios are nearly chondritic in the inclusions studied here (0.93–1.25 × C1), as in Allende inclusions (mean of 0.83 ± 0.05 × C1) in the ten of GROSSMAN and GANAPATHY (1976a) and GROSSMAN et al. (1977), strongly supporting the inferences of GROSSMAN et al. (1977) that Eu was divalent when it condensed from the solar nebula, and Eu and Sr were carried into CAIs by melilite. Eight of the ten refractory inclusions of this study, however, have unusual or unique refractory trace element characteristics compared to those seen in Allende inclusions. Particularly striking are the extraordinarily large concentrations of Re and Os (~57–145 × C1) in Vig1, L2, Ef1, and Ef2, which suggests that the total amount of hcp condensate metal alloy sampled by those inclusions is 4–9 times that sampled by most Allende inclusions. L1, L2, Vig1, Vig2, Ef1, and Ef2 have unusually large Os/Ru ratios (up to 6.9 × C1), suggesting that removal temperatures of hcp alloy precursors of these inclusions were unusually high (up to ~1655 K at 10^{-3} atm) compared to Allende inclusions. Unusual refractory lithophile element characteristics found in inclusions of this study include low Zr/Hf ratios (~0.4 × C1) in L2 and L4, possibly because of oversampling of zirconium oxide; low V/Yb ratios (~0.25 × C1) in L1 and Ef2, possibly because of oversampling of perovskite; a high Sr/Yb (~2.4 × C1) ratio in Ef2, probably because of oversampling of melilite; and high Hf/Lu (~2.6 × C1), Sc/Lu (~3.1 × C1), and Zr/Lu (~2.8 × C1) ratios in Ef3, probably because of oversampling of hibonite and/or zirconium oxide.

Of twenty-five inclusions from the reduced subgroup now studied in this laboratory (five by MAO et al., 1990; ten by SYLVESTER et al., 1992; ten here), seventeen have refractory element characteristics which are unusual or distinct from those in Allende inclusions. MAO et al. (1990) and SYLVESTER et al. (1992) found their unusual inclusions in Leoville and Vigarano. In this study, we have shown that Efremovka, too, contains unusual inclusions. A large proportion of inclusions in the reduced subgroup possess greater fractionations relative to C1 chondrites of refractory siderophiles from one another, of trace refractory lithophiles from one another, and of refractory siderophiles from trace refractory lithophiles than are found in Allende CAIs. Much of this we have attributed to preferential sampling of nebular host phases of some trace elements relative to others during accretion of inclusion precursors. Why did this happen to a greater degree in the region where CAIs of the reduced subgroup formed than where Allende CAIs formed? The host phases of refractory trace elements were at least partially separated spatially from one another in both regions but the mixture of these phases apparently was not as vigorously stirred in the region where CAIs of the reduced subgroup formed as where those in Allende did, pointing to possible differences in the intensity

and/or type of gas-grain separation processes in the two regions. It seems clear that C3V chondrites of the reduced subgroup sampled parts of the nebula which were not well sampled by Allende, a member of the oxidized subgroup. What is less clear, and what future studies should attempt to determine, is whether it is only Allende which did not sample a wide variety of early nebular assemblages, or whether this is a characteristic common to all members of the oxidized subgroup.

Like most coarse-grained inclusions from the reduced subgroup studied previously, most of those analyzed here have lower concentrations of Na, Au, Fe, Zn, and Mn than their Allende counterparts. This is consistent with the idea that they experienced secondary alteration at a higher temperature or for a shorter time than Allende inclusions. The fine-grained Leoville inclusion studied here has lower concentrations of nonrefractory elements than Allende fine-grained inclusions, as is the case for another fine-grained Leoville inclusion analyzed by MAO et al. (1990). Unlike Vigarano fine-grained inclusions (SYLVESTER et al., 1992), those in Leoville experienced secondary alteration at a higher temperature or for a shorter time than Allende fine-grained inclusions.

Acknowledgments—We are grateful to J. R. Beckett and R. C. Newton for advice about thermodynamic data, J. M. Lattimer for performing condensation calculations, T. P. Ward for assistance with the rabbit irradiation, S. Yoneda for assistance in data reduction, A. M. Davis for helpful discussions, and J. R. Beckett, J. W. Larimer, and R. A. Schmitt for constructive reviews. This research was supported by funds from the National Aeronautics and Space Administration through grant NAG 9-54.

Editorial handling: R. A. Schmitt

REFERENCES

ANDERS E. and GREVESSE N. (1989) Abundances of the elements: Meteoritic and solar. *Geochim. Cosmochim. Acta* **53**, 197–214.

BECKETT J. R. (1986) The origin of calcium-, aluminum-rich inclusions from carbonaceous chondrites: an experimental study. Ph.D. thesis, Univ. Chicago.

BISCHOFF A., PALME H., and SPETTEL B. (1987) A37—A coarse-grained, volatile element-poor, Ca, Al-rich inclusion with huge Fremdlinge. *Lunar Planet. Sci. XVIII*, 81–82 (abstr.).

BOYNTON W. V. (1975) Fractionation in the solar nebula: Condensation of yttrium and the rare earth elements. *Geochim. Cosmochim. Acta* **39**, 569–584.

BOYNTON W. V., WARK D. A., and ULYANOV A. A. (1986) Trace elements in Efremovka fine-grained inclusion E14: Evidence for high temperature, oxidizing fractionations in the solar nebula. *Lunar Planet. Sci. XVII*, 78–79 (abstr.).

CHAMBERLIN L., BECKETT J. R., and STOLPER E. M. (1991) Experimental determination of the free energy of formation of $MgAl_2O_4$ spinel: an important constraint on solar system processes. *Lunar Planet. Sci. XXII*, 195–196 (abstr.).

CONARD R. (1976) A study of the chemical composition of Ca-Al-rich inclusions from the Allende meteorite. M.S. thesis, Oregon State Univ.

DAVIS A. M. (1991) Ultrarefractory inclusions and the nature of the group II REE fractionation. *Meteoritics* **26**, 330 (abstr.).

DAVIS A. M. and GROSSMAN L. (1979) Condensation and fractionation of rare earths in the solar nebula. *Geochim. Cosmochim. Acta* **43**, 1611–1632.

DAVIS A. M., GROSSMAN L., and ALLEN J. M. (1978) Major and trace element chemistry of separated fragments from a hibonite-bearing Allende inclusion. *Proc. 9th Lunar Planet. Sci. Conf.*, 1235–1247.

DAVIS A. M., TANAKA T., GROSSMAN L., LEE T., and WASSERBURG G. J. (1982) Chemical composition of HAL, an isotopically-unusual Allende inclusion. *Geochim. Cosmochim. Acta* **46**, 1627–1651.

EKAMBARAM V., KAWABE I., TANAKA T., DAVIS A. M., and GROSSMAN L. (1984) Chemical compositions of refractory inclusions in the Murchison C2 chondrite. *Geochim. Cosmochim. Acta* **48**, 2089–2105.

FAHEY A. J., GOSWAMI J. N., MCKEEGAN K. D., and ZINNER E. (1987) ^{26}Al, ^{244}Pu, ^{50}Ti, REE and trace element abundances in hibonite grains from CM and CV meteorites. *Geochim. Cosmochim. Acta* **51**, 329–350.

FEGLEY B., JR., and PALME H. (1985) Evidence for oxidizing conditions in the solar nebula from Mo and W depletions in refractory inclusions in carbonaceous chondrites. *Earth Planet. Sci. Lett.* **72**, 311–326.

GEIGER C. A., KLEPPA O. J., MYSEN B. O., LATTIMER J. M., and GROSSMAN L. (1988) Enthalpies of formation of $CaAl_4O_7$ and $CaAl_{12}O_{19}$ (hibonite) by high temperature, alkali borate solution calorimetry. *Geochim. Cosmochim. Acta* **52**, 1729–1736.

GLADNEY E. S., BURNS C. E., and ROELANDTS I. (1983) 1982 compilation of elemental concentrations in eleven United States Geological Survey rock standards. *Geostand. Newsl.* **7**, 3–226.

GRAHAM A. L. (1975) The Allende meteorite: Chondrule composition and the early history of the solar system. *Smithson. Contrib. Earth Sci.* **14**, 35–40.

GRAY C. M. and COMPSTON W. (1974) Excess ^{26}Mg in the Allende meteorite. *Nature* **251**, 495–497.

GROSSMAN L. (1972) Condensation in the primitive solar nebula. *Geochim. Cosmochim. Acta* **36**, 597–619.

GROSSMAN L. (1975) Petrography and mineral chemistry of Ca-rich inclusions in the Allende meteorite. *Geochim. Cosmochim. Acta* **39**, 433–454.

GROSSMAN L. (1977) Chemical fractionation in the solar nebula. In *The Soviet-American Conference on Cosmochemistry of the Moon and Planets* (ed. J. H. POMEROY and N. J. HUBBARD); *NASA SP-370*, pp. 787–796. US Gov't Print. Off.

GROSSMAN L. (1980) Refractory inclusions in the Allende meteorite. *Ann. Rev. Earth Planet. Sci.* **8**, 559–608.

GROSSMAN L. and CLARK S. P., JR. (1973) High-temperature condensates in chondrites and the environment in which they formed. *Geochim. Cosmochim. Acta* **37**, 635–649.

GROSSMAN L. and GANAPATHY R. (1975) Volatile elements in Allende inclusions. *Proc. 6th Lunar Sci. Conf.*, 1729–1736.

GROSSMAN L. and GANAPATHY R. (1976a) Trace elements in the Allende meteorite: I. Coarse-grained, Ca-rich inclusions. *Geochim. Cosmochim. Acta* **40**, 331–344.

GROSSMAN L. and GANAPATHY R. (1976b) Trace elements in the Allende meteorite: II. Fine-grained, Ca-rich inclusions. *Geochim. Cosmochim. Acta* **40**, 967–977.

GROSSMAN L., GANAPATHY R., and DAVIS A. M. (1977) Trace elements in the Allende meteorite: III. Coarse-grained inclusions revisited. *Geochim. Cosmochim. Acta* **41**, 1647–1664.

HASHIMOTO A. (1992) The effect of H_2O gas on volatilities of planet-forming major elements: I. Experimental determination of thermodynamic properties of Ca-, Al-, and Si-hydroxide gas molecules and its application to the solar nebula. *Geochim. Cosmochim. Acta* **56**, 511–532.

HINTON R. W., DAVIS A. M., SCATENA-WACHEL D. E., GROSSMAN L., and DRAUS R. J. (1988) A chemical and isotopic study of hibonite-rich refractory inclusions in primitive meteorites. *Geochim. Cosmochim. Acta* **52**, 2573–2598.

IRELAND T. R., FAHEY A. J., and ZINNER E. K. (1988) Trace-element abundances in hibonites from the Murchison carbonaceous chondrite: Constraints on high-temperature processes in the solar nebula. *Geochim. Cosmochim. Acta* **52**, 2841–2854.

KAWABE I., TANAKA T., EKAMBARAM V., DAVIS A. M., and GROSSMAN L. (1986) INAA determination of holmium in submilligram samples of cosmochemical and geochemical interest and the second-order activation interference. *J. Radioanal. Nucl. Chem.* **102**, 227–238.

KERRIDGE J. F. (1981) Compositions of calcium, aluminum-rich inclusions: constraints on models of nebular condensation. *Lunar Planet. Sci. XII*, 534–536 (abstr.).

KUEHNER S. M., LAUGHLIN J. R., GROSSMAN L., JOHNSON M. L., and BURNETT D. S. (1989) Determination of trace element mineral/liquid partition coefficients in melilite and diopside by ion and electron microprobe techniques. *Geochim. Cosmochim. Acta* **53**, 3115–3130.

LATTIMER J. M. and GROSSMAN L. (1978) Chemical condensation sequences in supernova ejecta. *The Moon and the Planets* **19**, 169–184.

MACPHERSON G. J. and GROSSMAN L. (1984) "Fluffy" Type A Ca-, Al-rich inclusions in the Allende meteorite. *Geochim. Cosmochim. Acta* **48**, 29–46.

MACPHERSON G. J., GROSSMAN L., ALLEN J. M., and BECKETT J. R. (1981) Origin of rims on coarse-grained inclusions in the Allende meteorite. *Proc. 12th Lunar Planet. Sci. Conf.*, 1079–1091.

MACPHERSON G. J., WARK D. A., and ARMSTRONG J. T. (1988) Primitive material surviving in chondrites: refractory inclusions. In *Meteorites and the Early Solar System* (ed. J. F. KERRIDGE and M. S. MATTHEWS), pp. 746–807. Univ. Arizona Press.

MAO X.-Y., WARD B. J., GROSSMAN L., and MACPHERSON G. J. (1990) Chemical compositions of refractory inclusions from the Vigarano and Leoville carbonaceous chondrites. *Geochim. Cosmochim. Acta* **54**, 2121–2132.

MASON B. and MARTIN P. M. (1977) Geochemical differences among components of the Allende meteorite. *Smithson. Contrib. Earth Sci.* **19**, 84–95.

MASON B. and TAYLOR S. R. (1982) Inclusions in the Allende meteorite. *Smithson. Contrib. Earth Sci.* **25**, 1–30.

MCGUIRE A. V. and HASHIMOTO A. (1989) Origin of zoned fine-grained inclusions in the Allende meteorite. *Geochim. Cosmochim. Acta* **53**, 1123–1133.

MCSWEEN H. Y., JR. (1977) Petrographic variations among carbonaceous chondrites of the Vigarano type. *Geochim. Cosmochim. Acta* **41**, 1777–1790.

NAZAROV M. A., ULYANOV A. A., KORINA M. I., and KOLESOV G. M. (1982) Efremovka CAI's: Major and trace element chemistry. *Lunar Planet. Sci. XIII*, 584–585 (abstr.).

NAZAROV M. A., BRANDSTÄTTER F., ULYANOV A. A., KOLESOV G. M., and KURAT G. (1987) Metal-rich CAI's in Efremovka (C3). *Lunar Planet. Sci. XVIII*, 702–703 (abstr.).

PALME H. and WLOTZKA F. (1979) A Ca, Al-rich inclusion from the Leoville (C3V)-meteorite. *Meteoritics* **14**, 508–511 (abstr.).

PALME H., LARIMER J. W., and LIPSCHUTZ M. E. (1988) Moderately volatile elements. In *Meteorites and the Early Solar System* (ed. J. F. KERRIDGE and M. S. MATTHEWS), pp. 436–461. Univ. Arizona Press.

PERLMAN I. and ASARO F. (1969) Pottery analysis by neutron activation. *Archaeometry* **11**, 21–52.

PERLMAN I. and ASARO F. (1971) Pottery analysis by neutron activation. In *Science and Archaeology* (ed. R. H. BRILL), pp. 182–195. MIT Press.

PERNICKA E. and WASSON J. T. (1987) Ru, Re, Os, Pt, and Au in iron meteorites. *Geochim. Cosmochim. Acta* **51**, 1717–1726.

ROBIE R. A., HEMINGWAY B. S., and FISHER J. R. (1978) Thermodynamic properties of minerals and related substances at 298.15K and 1 bar (10^5 pascals) pressure and at higher temperatures. *USGS Bull. 1452*.

ROBINSON G. R., JR., HAAS J. L., JR., SCHAFER C. M., and HASELTON H. T., JR. (1982) Thermodynamic and thermophysical properties of selected phases in the MgO-SiO_2-H_2O-CO_2, CaO-Al_2O_3-SiO_2-H_2O-CO_2, and Fe-FeO-Fe_2O_3-SiO_2 chemical systems, with special emphasis on the properties of basalts and their mineral components. *USGS Open-File Report 83-79*.

SIMON S. B. and GROSSMAN L. (1991) Petrography of a suite of refractory inclusions from the Leoville, Efremovka and Vigarano carbonaceous chondrites. *Lunar Planet. Sci. XXII*, 1261–1262 (abstr.).

SIMON S. B. and GROSSMAN L. (1992) Low-temperature exsolution in refractory siderophile element-rich opaque assemblages from the Leoville carbonaceous chondrite. *Earth Planet. Sci. Lett.* **110**, 67–75.

SIMON S. B., GROSSMAN L., and DAVIS A. M. (1991) Fassaite composition trends during crystallization of Allende Type B refractory inclusion melts. *Geochim. Cosmochim. Acta* **55**, 2635–2655.

STOLPER E. (1982) Crystallization sequences of Ca-Al-rich inclusions from Allende: An experimental study. *Geochim. Cosmochim. Acta* **46**, 2159–2180.

SYLVESTER P. J. and GROSSMAN L. (1991) Chemical compositions of refractory inclusions from Leoville, Efremovka and Vigarano. *Lunar Planet. Sci. XXII*, 1369–1370 (abstr.).

SYLVESTER P. J., WARD B. J., GROSSMAN L., and HUTCHEON I. D. (1990) Chemical compositions of siderophile element-rich opaque assemblages in an Allende inclusion. *Geochim. Cosmochim. Acta* **54**, 3491–3508.

SYLVESTER P. J., GROSSMAN L., and MACPHERSON G. J. (1992) Refractory inclusions with unusual chemical compositions from the Vigarano carbonaceous chondrite. *Geochim. Cosmochim. Acta* **56**, 1343–1363.

WARK D. A. (1981) The pre-alteration compositions of Allende Ca-Al-rich condensates. *Lunar Planet. Sci. XII*, 1148–1150 (abstr.).

WARK D. A. (1986) Evidence for successive episodes of condensation at high temperature in a part of the solar nebula. *Earth Planet. Sci. Lett.* **77**, 129–148.

WARK D. A. and BOYNTON W. V. (1983) The Scorpion, a novel spinel-hibonite-melilite inclusion in the Allende meteorite. *Lunar Planet. Sci. XIV*, 826–827 (abstr.).

WARK D. A. and LOVERING J. F. (1977) Marker events in the early solar system: Evidence from rims on Ca-Al-rich inclusions in carbonaceous chondrites. *Proc. Lunar Sci. Conf.*, 95–112.

WARK D. A. and LOVERING J. F. (1982) The nature and origin of type B1 and B2 Ca-Al-rich inclusions in the Allende meteorite. *Geochim. Cosmochim. Acta* **46**, 2581–2594.

WASSON J. T., OUYANG X., WANG J., and JERDE E. (1989) Chemical classification of iron meteorites: XI. Multi-element studies of 38 new irons and the high abundance of ungrouped irons from Antarctica. *Geochim. Cosmochim. Acta* **53**, 735–744.